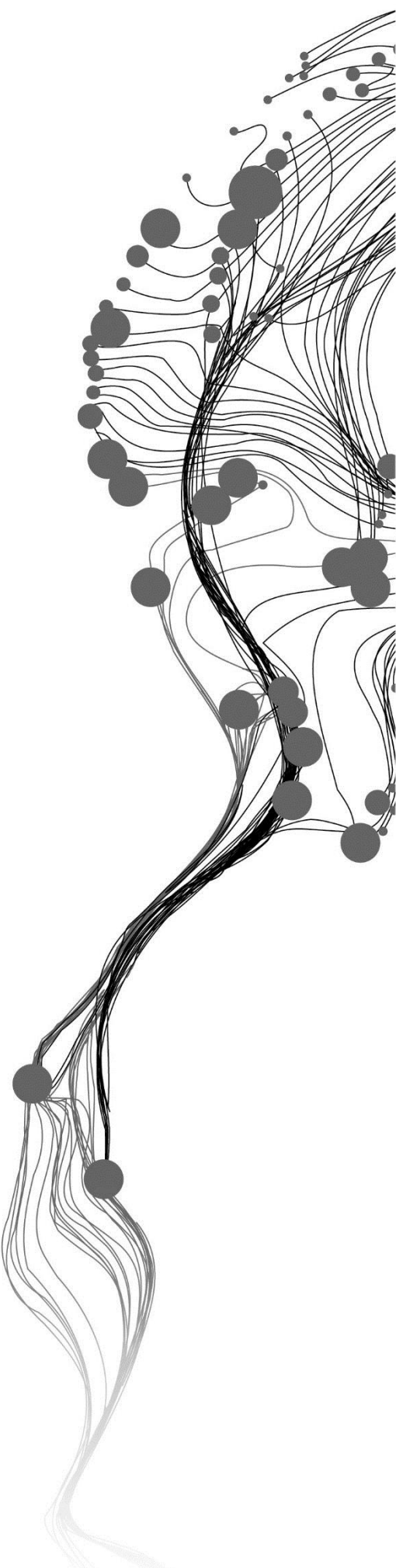


**USE OF SATELLITE DATA TO
MONITOR URBAN WATER
MANAGEMENT
INFRASTRUCTURES UNDER
EXTREME WEATHER
CONDITIONS: PRELIMINARY
STUDY**

CHAO MAI
March, 2015

SUPERVISORS:
Dr.Ir. C.M.M. Mannaerts (Chris)
Dr. Y. Zeng (Yijian)



USE OF SATELLITE DATA TO MONITOR URBAN WATER MANAGEMENT INFRASTRUCTURES UNDER EXTREME WEATHER CONDITIONS: PRELIMINARY STUDY

CHAO MAI

Enschede, The Netherlands, March, 2015

Thesis submitted to the Faculty of Geo-Information Science and Earth Observation of the University of Twente in partial fulfilment of the requirements for the degree of Master of Science in Geo-information Science and Earth Observation.

Specialization: Water Resources and Environmental Management

THESIS ASSESSMENT BOARD:

Dr. Ir. M.S. Salama (Chair)

Ir. J. van der Scheer (External Examiner, Waterschap Vechtstromen)

Dr.Ir. C.M.M. Mannaerts

Dr. Y. Zeng

DISCLAIMER

This document describes work undertaken as part of a programme of study at the Faculty of Geo-Information Science and Earth Observation of the University of Twente. All views and opinions expressed therein remain the sole responsibility of the author, and do not necessarily represent those of the Faculty.

ABSTRACT

As the frequency of extreme rainfall is increasing in Europe, it causes countless damage to human beings. One of solution to manage excess water is constructed wetlands, which can be used as water storage and water purification. “Kristalbad” is such kind of new infrastructure located between Enschede and Hengelo (Dutch cities). This study focused on how to use remote sensing (RS) to get the extreme weather conditions (rain rate, cloud properties), to derive surface properties (distribution of paved, unpaved, water bodies, sewer, seepage, etc.) and to generate input data for a simulation model (DMS) of the hydrology and hydraulic processes (runoff, discharge, etc.). It contains several parts such as deriving rain rate from satellite image, building a sub-catchment based on digital elevation model (DEM) and developing a prototype model (RAM-Duflow) to monitor the runoff, and flows through the constructed wetlands.

Meteosat second generation (MSG) was first introduced to get the rain rate while it gave underestimated results. From the literature review, it can be found that cloud microphysical properties can be related to precipitation detection. The cloud physical propertied (CPP) algorithms were used here which is based on cloud water path (CWP), cloud top temperature (CTT), cloud effective drop radius (CRE) and cloud optical thickness(COT) to estimate rain rate. It shows relative good results after calibration by in-situ data compared with the result obtained from an older Auto-estimator (AE) algorithm which is only based on CTT.

Different remote sensing elevation data were compared and evaluated for characterizing the drainage area and network. The Shuttle Radar Topographic Mission (SRTM) in the resolution of 30m and the Dutch official “Actueel Hoogtebestand Nederland” or (AHN), an airborne LIDAR based DEM, in resolutions of 5m and 0.5m. The results showed that the drainage network derived from 0.5m resolution gives a relatively good agreement when linked with the real drainage network.

Then the DMS (Duflow Modeling Studio) suite was evaluated for its use for modeling rainfall runoff and flows through the constructed Kristalbad wetland

Two simplified prototype models (a RAM component) and a Duflow network model were built using data from the Water authorities and our derived remote sensing data. The simplified “prototype” RAM – Duflow modeling was performed on the area in order to simulate the rainfall runoff. The DMS was run only in the RAM mode because of the complexity of the infrastructures and drainage systems, and also the limitation of the data. Results of the simulation indicate that RAM is a useful tool to compute rainfall runoff from user defined catchment areas. Although a first Duflow network schematization of the waste water treatment plant (WWTP) - Elsbeek to Kristalbad system was initiated, research time (at ITC < 6 months all in), did not permit to generate a full model set-up and perform modeling runs. We can recommend to continue the research with more detailed follow-up studies for setting up a full flow and water quality model of the system and verify the applicability of the DMS suite. Also the use of satellite data for monitoring and predicting extreme rainfall in the region could be further continued.

Keywords: Enschede, Netherlands, constructed wetlands, Meteosat MSG, CPP algorithm, DMS Duflow model

ACKNOWLEDGEMENTS

First of all, my deepest thanks to my father and my mother for their honorable support, encouragements and love.

I would like to appreciate ITC and Chang'an University to give me this opportunity to study at the Water resources department.

Special thanks to Dr. Chris Mannaerts, I appreciate the tremendous support and advices throughout the whole research period which have helped me a lot. To my second supervisor, Dr. Yijian Zeng, for his useful comments and advises that encouraged me during the entire period of my pursuance of the thesis. I also would like to express my gratefulness to Ir. J. van der Scheer for the help he provided me the very useful information about my study area.

I appreciate all my friends and classmates, our 11 person team from Chang'an University, other country mates I met in ITC and foreign friends from all over the world. I will never forget their support, friendship and very nice time that we were shared together at ITC.

Thanks to all ITC staff, especially to all staff in WREM, for the continuous and important support during my study. I learned a lot from their advanced demonstration, lectures and classes.

TABLE OF CONTENTS

1.	Introduction.....	9
1.1.	Background.....	9
1.2.	Research problem.....	9
1.3.	Research Objectives.....	10
1.4.	Research Questions.....	10
1.5.	Study Area Description.....	10
1.6.	Climate.....	11
1.6.1.	Temperature.....	11
1.6.2.	Precipitation and Evaporation.....	12
2.	Materials.....	13
2.1.	Remote sensing data.....	13
2.1.1.	Meteosat second generation (MSG).....	13
2.1.2.	Royal Netherlands Meteorological Institute (KNMI).....	14
2.1.3.	Shuttle Radar Topographic Mission (SRTM).....	14
2.1.4.	Actueel Hoogtebestand Nederland (AHN).....	14
2.2.	Data collection from water authority.....	15
2.2.1.	Stream section details.....	15
2.2.2.	Other in-situ data.....	15
3.	Integration of satellite remote sensing data.....	17
3.1.	Rain rate estimation from space.....	17
3.2.	Cloud properties under extreme rainfall.....	21
3.2.1.	Introduction.....	21
3.2.2.	Methods.....	22
3.2.3.	Data preparation.....	23
3.2.4.	Data processing.....	23
3.2.5.	Data extraction.....	27
3.2.6.	Data analysis.....	28
3.2.7.	Discussion.....	30
3.3.	Regional occurrence of extreme rainfall.....	31
4.	DEM data process and analysis.....	33
4.1.	Two resources of near global elevation data sets.....	33
4.1.1.	Shuttle Radar Topographic Mission (SRTM) based DEM.....	33
4.1.2.	Actual Height Netherlands (AHN) based DEM.....	33
4.2.	Data processing.....	34
4.3.	LULC reclassification.....	37
5.	Hydrodynamic Modeling.....	41
5.1.	Duflow Modeling Studio (DMS).....	41
5.2.	Duflow model.....	41
5.3.	Duflow rainfall runoff (RAM) component.....	42
5.3.1.	Open water surface.....	43
5.3.2.	Paved surface.....	44
5.3.3.	Unpaved surfaces.....	45
5.4.	Previous modeling studies with Duflow.....	46
5.5.	Model simplifications and limitations.....	47
6.	Simplified “Prototype” Duflow–RAM modeling.....	49
6.1.	Modeling objectives.....	49
6.2.	Schematization of the study area.....	49

6.3.	Precipitation and Evaporation	50
6.4.	Initial and Boundary conditions.....	51
6.5.	RAM simulation result.....	52
7.	Conclusions and recommendations.....	55
7.1.	Overall conclusions.....	55
7.2.	Recommendations.....	57
	References.....	58
	Appendix.....	62

LIST OF FIGURES

Figure 1-1 Geographical location of the Kristalbad	11
Figure 1-2 Monthly average precipitation and evapotranspiration data from Twente station	12
Figure 2-1 KNMI meteorological stations.....	14
Figure 3-1 Enschede sub-catchment with 6 points overlaid on top of MSG MPE image (20/06/2013)	19
Figure 3-2 Comparison the data of MSG and gauge stations	20
Figure 3-3 MSG data ordering window	23
Figure 3-4 Example of using “gdalinfo” to check CTH data	24
Figure 3-5 Example of processed CTH image on June 20th 2013	25
Figure 3-6 Example of using “gdalinfo” to check OCA raw data.....	26
Figure 3-7 Example of processed OCA image on June 20th 2013	27
Figure 3-8 Example of using MSG Data Retriever to get CTT value.....	27
Figure 3-9 Comparison between CTT and CTH	28
Figure 3-10 Comparison of CTH retrieved from MSG and calibrated CTH using equation 3-5.	28
Figure 3-11 Rainfall (mm/h) derived from CPP (left) and AE (right) algorithms on 20th June 2013, 13:00-15:00 UTC.....	30
Figure 3-12 CPP and AE compared to observed rain gauge measurements on 20th June 2013	30
Figure 3-13 Times of rainfall larger than R99T (heavy rainfall) and R99.9T (extreme rainfall).....	32
Figure 3-14 Max daily rainfall in every year	32
Figure 3-15 Frequency analysis.....	32
Figure 4-1 AHN-units map display by ILWIS	34
Figure 4-2 DEM hydro-processing procedure for drainage network and sub-catchment extraction.....	35
Figure 4-3 Sub-catchment for SRTM based DEM (spatial resolution: 30m).....	36
Figure 4-4 Sub-catchment for AHN based DEM (spatial resolution: 5m and 0.5m respectively)	36
Figure 4-5 SRTM (30m) based drainage network (left) compared with AHN (5m) based drainage network	37
Figure 4-6 AHN 5m (left) vs. 0.5m (right) resolution based drainage network	37
Figure 4-7 Example of TOP10NL map download from PDOK, layout scale 1:50,000	38
Figure 4-8 LULC map extract from TOP10NL.....	38
Figure 4-9 Reclassification map and properties of the sub-catchment.....	39
Figure 5-1 Duflow RAM modeling framework	43
Figure 6-1 Percentage of each categories	50
Figure 6-2 Time relate graph of precipitation and evaporation (mm/day) for RAM.....	51
Figure 6-3 Urban surface characteristic	52
Figure 6-4 Unpaved surface scheme setting for study area.....	52
Figure 6-5 Discharge computed from RAM module.....	53
Figure 7-1 Example of network for Kristalbad.....	57

LIST OF TABLES

Table 1-1 Monthly average temperature	11
Table 1-2 Monthly average precipitation and evapotranspiration	12
Table 2-1 Characteristics of 12 SEVIRI imaging Channels	13
Table 3-1 IR versus MV	18
Table 3-2 Cumulative rainfall figures	19
Table 3-3 Cloud properties	23
Table 3-4 OCA parameters	26
Table 3-5 Statistical analysis of results on 20th June between the algorithms of the day's total estimates	30
Table 3-6 Relative frequency of heavy rainfall and extreme rainfall	32
Table 4-1 SRTM data format	33
Table 4-2 AHN data format	34
Table 4-3 Sub-catchment properties from each DEM	37
Table 4-4 Reclassifications of land cover classes for modeling	39

LIST OF APPENDICES

Appendix 1 Raw data import into ILWIS format.....	62
Appendix 2 Map calculation	62
Appendix 3 Rain rate (mm/h) of each point retrieved from MSG on June 20 th 2013	63
Appendix 4 Rain rate (mm/h) retrieved from AE and CPP during daylight	63
Appendix 5 Rain rate, level and discharge data for WWTP (source: Water authority)	63
Appendix 6 Inlet of level and discharge data for Kristalbad (source: Water authority)	65
Appendix 7 Outlet of level data (source: Water authority).....	66
Appendix 8 More details about Kristalbad.....	67

ABBREVIATIONS

AE	Auto-estimator of precipitation
AHN	Digital elevation data for the Netherlands
COT	Cloud Optical Thickness
CPP	Cloud Physical Properties
CRE	Cloud Effective Radius
CTH	Cloud Top Height
CTP	Cloud Top Pressure
CTT	Cloud Top Temperature
CWP	Cloud Water Path
DEM	Digital Elevation Model
DMS	Duflow Modelling Studio
EUMETSAT	European Organization for the Exploitation of Meteorological Satellites
ILWIS	Integrated Land and Water Information System
IR	Infra-red band
ITC	International Institute for Geo-Information Science and Earth Observation
KNMI	Royal Netherlands Meteorological Institute
LULC	Land Use and Land Cover
LWP	Liquid Water Path
MPE	Multi-sensor Precipitation Estimate
MSG	Meteosat Second Generation
MV	Microwave band
NIR	Near-infrared band
OCA	Optimal Cloud Analysis
RAM	Precipitation Runoff Module
R99T	99th Percentiles
RMSE	Root Mean Square Error
SEVIRI	Spinning Enhanced Visible and Infrared Instrument
SRTM	Shuttle Radar Topographic Mission
TOP10NL	Digital Topographic file of the Netherlands
UMARF	Unified Meteorological Archive and Retrieval Facility
VIS	Visible band
WWTP	Waste Water Treatment Plant

1. INTRODUCTION

1.1. Background

Constructed wetlands have been increasingly used throughout the world for water storage and treatment. Conventional biological wastewater treatment systems presents some drawbacks such as high economic costs (activated sludge or trickling filters) for small communities and low treatment efficiencies (collective septic tanks). By contrast, natural treatment system such as constructed wetlands have more advantages like low energy requirements, straightforward operation, maintenance works (Arroyo et al, 2013) and higher efficiency than other systems (algae-based systems) (García et al. 2008). Moreover, it also enhances the aesthetic feeling of the surrounding landscape and provides a good habitat for many aquatic organisms.

The “Kristalbad” is a recently constructed artificial wetland infrastructure for local flood water storage and control (and pollutant removal) of urban runoff waters from Enschede city area. It is intended to protect downstream areas (Hengelo city and surroundings) from high storm water runoffs and loadings, resulting from local extreme rainfalls over the urban area and surroundings. Being a wetland type of facility, additional removal of suspended solids, nutrients such as carbon (C), nitrogen (N), phosphorus (P), micro-substances, and heavy metals from the runoff stream is a possible positive side effect of the flood water control structure. Next to these functions, the Kristalbad was also built to generate a “green corridor” between Enschede and Hengelo city areas, as well as for recreational (walking, bird watching, etc.) and aesthetic surrounding purposes.

1.2. Research problem

It is well-known that global warming will lead to more evaporation and a higher intensity of water cycling as reported by the European Commission (Rutger & Rpland, 2008). A warmer atmosphere can store more water vapor and a higher energy potential. As a result of this natural phenomenon, the intensity and frequency of extreme events will increase (Becker & Grünwald, 2003; Hartmann et al., 2013). This increase may generate a great change than average data, but also have possibility of duration of little precipitation longer than usual. Previous studies of extreme precipitation in Europe corroborate this trend (Semmler & Jacob, 2004; Beniston et al., 2007).

Extreme rainfall events cause countless damage to properties, public infrastructure, agriculture, and tourism in many cities. Storm water runoff often contains significant loads of pollutants, such as litter, oils, heavy metals, sediment, nutrients, organic matter and micro-organisms (Davies & Bavor, 2000), which will have considerable impacts on urban drainage systems and receiving natural aquatic water systems.

Thus it is important to find ways to measure and simulate the excess water, which may affect the functioning of the “Kristalbad”.

1.3. Research Objectives

The objective of this research is to assess the use of remote sensing data for monitoring urban water management infrastructures under extreme rainfall condition.

- To review and characterize local weather conditions and occurrences of extreme rainfalls for the study area
- To evaluate of the weather satellite and in-situ data for tracking and determining extreme rainfall rates in time and space
- To perform the DEM hydro-processing to urban and semi-urban areas and determine the optimized spatial resolution
- To build a prototype hydraulic model to simulate extreme rainfall for the study area and the Kristalbad constructed wetlands
- To give guidelines to further analyze the hydraulic and hydrologic behavior of the Kristalbad using a model-based approach.

1.4. Research Questions

The objectives mentioned above, the data to be collected and the methods selected will address the following formulated research questions.

- What is the behavior of the extreme events occurrence/ frequency?
- How do MSG (SEVIRI) and derived rainfall data correlate with KNMI and in-situ gauge rainfall data for extreme rainfall respectively?
- Whether the use of higher spatial resolution image will provide significant differences in results?
- Can extreme rainfall runoff flows be simulated using a simplified urban system model approach (e.g. DMS-RAM)?
- Is a DMS model useful to analyze the Kristalbad function during extreme precipitation event?

1.5. Study Area Description

Enschede is a municipality and a city in the eastern Netherlands in the province of Overijssel and in the Twente region. It has approximately a population of 160,000 with in an area of 142.72 km². Hengelo city is in the northwest of Enschede, there is a considerable height difference between Hengelo of elevation 18 m and Enschede of elevation 42 m above mean sea level.

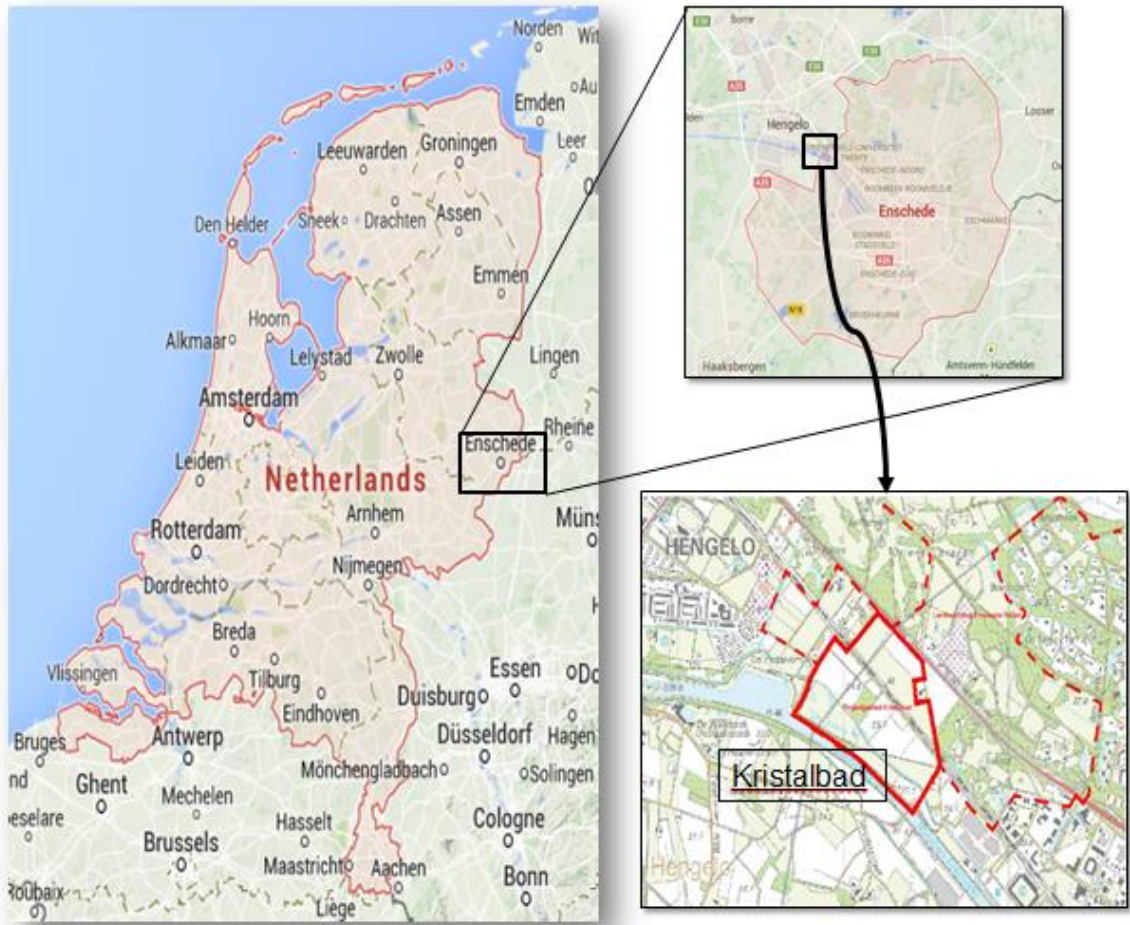


Figure 1-1 Geographical location of the Kristalbad

Kristalbad, a complex constructed wetland area of 40 hectares lies on the border of the municipalities of Enschede and Hengelo, Netherlands, north of the Twente Canal and south of the Hengelo street / Enschede street. The railroad Hengelo-Enschede bisects the area. It is situated between latitudes 52°14'29" to 52°14'50"N and longitudes 6°49'08" to 6°49'45"E. Its altitude ranges from about 21 m to 24 m above sea level. After construction of the retention area, the Kristalbad can store 187000 cubic meters of water in times of high rainfall.

1.6. Climate

1.6.1. Temperature

Like most of the Netherlands, Enschede and Hengelo features an oceanic climate (Cfb), defined by the Köppen Climate Classification (Peel et al. 2007). The generally features warm (but not hot) summers and cool (but not cold) winters. The table 1-1 lists the daily temperature data of Twente station (1981-2010) were collected from Royal Netherlands Meteorological Institute (KNMI). The annual mean temperature ranges from 6 °C to 13 °C.

Table 1-1 Monthly average temperature

Temperature data for Twente (1981-2010)													
Month	January	February	March	April	May	June	July	August	September	October	November	December	Year
Average high °C	4.8	5.7	9.5	13.9	18.0	20.5	22.8	22.5	18.7	14.1	8.9	5.2	13.72
Daily mean °C	2.3	2.6	5.6	8.9	12.9	15.4	17.6	17.1	14.0	10.2	6.0	2.9	9.63
Average low °C	-0.5	-0.6	1.5	3.4	7.1	9.6	12.0	11.5	9.2	6.2	3.0	0.3	5.23

Source: KNMI

1.6.2. Precipitation and Evaporation

Daily precipitation and evaporation data of the year among 1981 to 2010 had been recorded in Twente station, as listed in table 1-2, the annual mean rainfall of the region is about 770 mm/year, and the annual evapotranspiration is about 460 mm. According to Figure 1-2 the distribution of monthly rainfall displays an even characteristic, but the evapotranspiration varies significantly, with high evaporation rates in summer than in winter.

Table 1-2 Monthly average precipitation and evapotranspiration

Month	January	February	March	April	May	June	July	August	September	October	November	December	Year
Precipitation (mm)	71.5	51.6	65.1	45.2	62.4	67.7	74.5	71.0	65.4	67.5	68.9	74.1	784.9
ETo(mm)	7.43	14.26	31.22	57.45	83.39	89.57	95.07	78.98	48.66	26.93	10.56	5.89	457.8

Source: KNMI

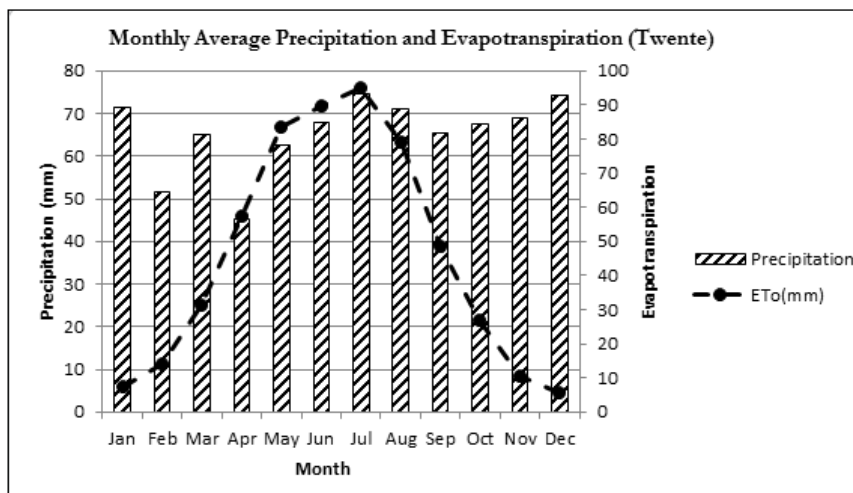


Figure 1-2 Monthly average precipitation and evapotranspiration data from Twente station

2. MATERIALS

For this thesis, there are 3 main sources for the data collection. One is GEONETCast and data archives internet (EUMETSAT, KNMI, SRTM, AHN and ITC database) for the climate and DEM data. Another is the water authority for hydraulic and hydrological data.

2.1. Remote sensing data

2.1.1. Meteosat second generation (MSG)

MSG was launched on 28 August 2002 by Europe Space Agency (ESA), it monitors a quarter of the Earth and its atmosphere from a fixed position in a geostationary position at 0° longitude, 35 800 km above the Gulf of Guinea off the west coast of equatorial Africa (“Meteosat Second Generation,” n.d.). Spinning Enhanced Visible and Infrared Instrument (SEVIRI) radiometer on board MSG provides more condensed information, it scans every 15 min and measure reflected and emitted radiance in 12 channels , three channels at visible and very near infrared wavelengths (between 0.6 and 1.6 μm), eight from near-infrared to thermal infrared wavelengths (between 3.9 and 14 μm), and one high-resolution visible channel. Each of the wavelengths has unique capabilities of reflecting certain characteristics of the clouds, the table below list a brief introduction for each channel and their respective applications.

Table 2-1 Characteristics of 12 SEVIRI imaging Channels

Channel	Name	Central wavelength (μm)	Applications
01	VIS 0.6	0.635	Cloud detection, land surface monitoring
02	VIS 0.8	0.81	
03	NIR 1.6	1.64	Distinguish between ice and water clouds
04	IR 3.9	3.9	Night detection of land sea temperature
05	WV 6.2	6.25	Measure water vapor content
06	WV 7.3	7.35	
07	IR 7.8	8.7	Information for thin cirrus clouds
08	IR 9.7	9.66	Responsive to ozone information
09	IR 10.8	10.8	Each responds to the temperature of clouds and surface
10	IR 12.0	12	
11	IR 13.4	13.4	CO ₂ absorption channel
12	HRV	0.4-1.1	High resolution VIS 0.6 channel

The nominal spatial resolution at the sub-satellite point is 1 by 1 km for the high-resolution channel, and 3 by 3 km for the other channels (D.M.A. Aminou, 2002 and Schmetz et al., 2002). Meteosat-9 (launched on 2005) provides the operational Europe Rapid Scanning Service (MSG-RSS), delivering more frequent images every five minutes over parts of Europe, Africa and adjacent seas. All MSG data are available from EUMETSAT. Data such as cloud top height

(CTH), cloud top temperature (CTT), atmospheric motion vectors (AMV), optimal cloud analysis (OCA) can be downloaded from MSG meteorological products extraction facility (MPEF).

2.1.2. Royal Netherlands Meteorological Institute (KNMI)

KNMI is the National Institute for Meteorology and Seismology, as well as a national reference institute (“KNMI,” n.d.). It operates 35 automatic weather stations (AWS) and provides daily data of temperature, sunshine, cloud cover and visibility, air pressure, wind and precipitation. Precipitation is measured using the KNMI rain gauge. This electric gauge is of a floating type and measures precipitation with a time resolution of 12 seconds (Brandsma, 2014). The hourly data is available via the KNMI website.

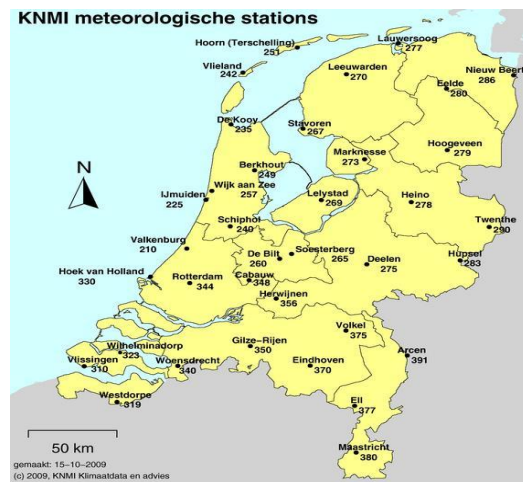


Figure 2-1 KNMI meteorological stations

2.1.3. Shuttle Radar Topographic Mission (SRTM)

The Shuttle Radar Topographic Mission created the complete, highest-resolution digital elevation model on a global scale (Farr et al., 2007). It was flown aboard the space shuttle Endeavour February 11-22, 2000. Endeavour orbited Earth 16 times each day during the 11-day mission. The elevation data sets provide global coverage from 60 degrees north to 56 degrees south latitude at 1 arc-second resolutions (approximately 30 meters). The data can be downloaded freely (<http://earthexplorer.usgs.gov/>).

2.1.4. Actueel Hoogtebestand Nederland (AHN)

The AHN Netherlands are files containing the Netherlands detailed digital elevation data. The height data was collected via Laser altimetry. It is a technique in which a plane or helicopter with a laser beam scans the surface, the duration of the laser reflection together with the aircraft position make the result more precise. Also the data can be downloaded freely (<https://www.pdok.nl/en>).

2.2. Data collection from water authority

The data which was collected from study area was basically used for calibration and validation of the rainfall and for the set-up of the models. The collected data helps to

- Define model input variables
- Define model parameters
- Assess the processes accuracy
- Verify the results

In this case, it is mainly used for reasoning out the physical process in the catchment system.

2.2.1. Stream section details

The stream section details are crucial information to define the simulated stream in Duflow. As we assume all stream sections are of the same shape and size between two nodes, the cross-section structure information must be known. Such data were also obtained from the water authority (Appendix 8).

2.2.2. Other in-situ data

In this research, the precipitation data (Appendix 5) from Municipal Waste Water Treatment Plant (WWTP) used as one of the required input parameters in RAM module. Other data set (Appendix 6 & 7) can be used for further study.

3. INTEGRATION OF SATELLITE REMOTE SENSING DATA

This chapter discuss in details the rainfall derived from different resources and cloud properties and occurrences of extreme rainfalls for the study area.

3.1. Rain rate estimation from space

Rainfall is produced in the lower atmosphere as a sequence of physical and chemical processes. The physics of precipitation is simplified in four parts. It occurs by air in clouds cooling to dew point temperature by vertical or forced uplift, condensation of water vapor, droplet growth and importation of water vapor. From these processes, some factors have significant effect on rainfall formation like cloud temperature, cloud phase (water or ice) and droplet properties. Fortunately, many of these parameters can be obtained from satellite images.

Although surface precipitation gauges that considered the normal and directly method for measuring rain rate, there are many areas that are not conveniently monitored. This includes the vast expanses of ocean and remote land areas. This kind of point measurement method also has many errors since it is affected by wind speed, distance to objects, evaporation, observer errors, etc. Nevertheless, the precipitation can also be observed by weather radars. And it is also possible to measure rainfall from space. Rainfall measurement from space are based on analysis of the solar radiation that is emitted or scattered from clouds, rainfall and ground surface. The radiation is recorded by the sensor which is installed in the satellite.

Rainfall satellite sensors in practice can be divided into 2 categories: Thermal infrared (IR) and microwave (MV) sensors.

- Infrared techniques depend on a wavelength window around 10-12 micron and give information about cloud tops. Basic assumption is that cloud-top temperature brightness is related to cloud height, which in turn is related to cloud thickness, and to rainfall rate. The Spinning Enhanced Visible and Infra-Red Imager (SEVIRI) which is on board the Meteosat Second Generation (MSG) satellite, is adept in detecting backscattered radiation from cloud tops in terms of brightness temperatures.
- Microwave sensors are the second category tools with potential to improve precipitation estimation. The sensor channels in the microwave part of the electromagnetic spectrum. The frequencies ranging from about 10 GHz to a few hundred GHz. The lower frequencies measure precipitation mainly from energy emitted by raindrops, while the higher frequencies gather energy scattered by ice particles above the freezing level. Satellites such as the Tropical Rainfall Measuring Mission (TRMM) and the Global Precipitation Measurement (GPM) mission are the common technologies for

precipitation estimates.

Table 3-1 IR versus MV

	IR	MV
Measuring object	Reflect cloud-top conditions only and thus are more weakly to measure wide range of conditions than MV radiances	Microwave radiances are more sensitive to moisture throughout the cloud
Time and space resolution	Data are available at 4km-1km resolution on geostationary platforms, allowing looks in many locations every 15 minutes	On the polar orbiting platforms, limiting views to 2 per day per satellite

Comparing with these two groups in Table 3-1, we found IR to be more suitable for small area and extreme precipitation events at short time scales; MV is more suitable large scales in time and space like the ocean. Thus a combination of these two satellite instruments for the estimation of precipitation is a favorable way to overcome the shortcoming of each measurement. In this case, EUMETSAT realized the Multi-sensor Precipitation Estimate (MPE) in order to achieve both the advantages of high temporal and space resolution from IR sensors and a better precision from microwave sensors (Heinemann, 2002).

3.1.1 MSG Multi-sensor Precipitation Estimate (MPE)

“The Multi-sensor Precipitation Estimate (MPE) is an instantaneous rain rate product which is derived from the IR-data of geo-stationary EUMETSAT satellite by continuous re-calibration of the algorithm with rain-rate data from polar orbiting microwave sensors”(Yucel & Onen, 2014). The data provided is the full earth scan every 15 minutes and the area rapid scan every 5 minutes. Currently METEOSAT-7, -8, -9 and -10 are being serviced for producing the real-time rainfall product.

The derivation of rain rates is based on the concept that cold clouds are more probable to produce raindrops than warmer clouds. The day 20th June 2013 with heavy rainfall in the study area was chosen in this research.

3.1.2 Data preparation

The data from the SEVIRI instrument are freely available for education and research, though efforts of the Group on Earth Observation (GEO), by means of their global data dissemination system – GEONETCast. More data have been imported and processed in this system. The routines developed also have been integrated into a Toolbox, called the “GEONETCast–Toolbox”, developed as a plug-in to be used within ILWIS.

From the “GEONETCast–Toolbox” main menu select “Meteorological Product Extraction Facility (MPEF)”, “High Temporal Resolution MPEF Products” and “MPEF MPEG” to import precipitation data. Select for the “Data” the identical time as used to import MSG images, in this case 20 June 2013, 00:00UTC.

- Time resolution : 15 minutes intervals (96 per day)
- Space resolution : 3×3 km² pixel size

The in-situ data from KNMI can freely be downloaded from the KNMI website. The hourly precipitation data are available since 1951 to now, hourly rainfall data for Twente region (code 290) were downloaded for the same days.

3.1.3 Data extraction

As specified in the previous section MPE data comes as HRIT file format and are connected with the Toolbox to ILWIS MPR file format in a layer stack. There are 96 MPR files on a certain day at 15 minutes time intervals. The image covers approximately half of the earth. So first, sub-maps were created for study area. Then 6 data extraction points have been selected considering the location of the sub-catchment and a point map was created and shown in Figure 3-1. In ILWIS, map list graph operation was used to extract the data from rainfall image stack which contains 96 layers.

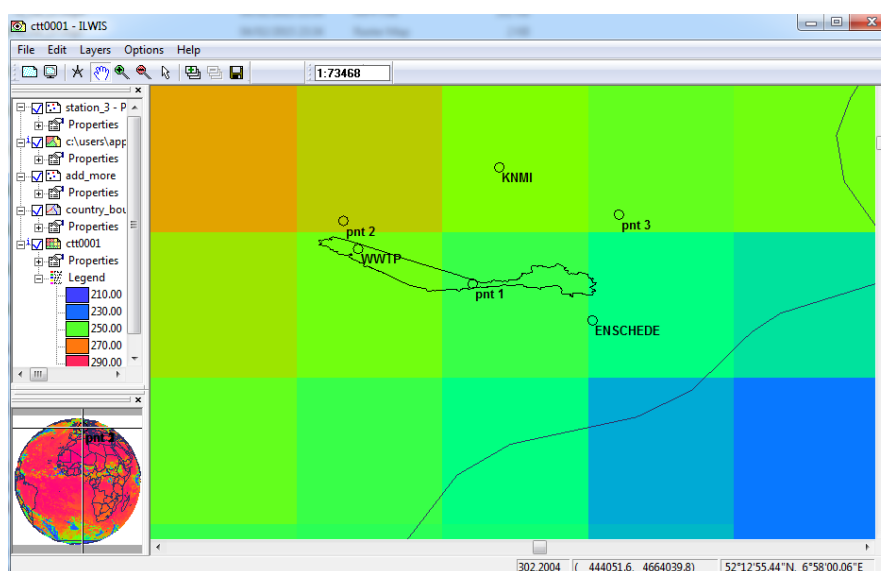


Figure 3-1 Enschede sub-catchment with 6 points overlaid on top of MSG MPE image (20/06/2013)

All 6 data extraction points are distributed as shown in Figure 3-1. The points were distributed evenly to cover the whole area of the sub-catchment. The point “KNMI” set at Twente airport which is the nearest point of the Twente station, and the point “WWTP” is the nearest point to the Kristalbad, other points information are shown in Table 3-2.

Table 3-2 Cumulative rainfall figures

Points	coordinates	Cumulative rainfall(mm)
Airport (KNMI)	(439230.7, 4666936.3)	20.9
WWTP	(436354.6, 4665283.6)	18.2
ENSCHEDÉ	(441155.3, 4663826.0)	16.1
Pnt 1	(438706.0, 4664564.7)	19.3
Pnt 2	(436004.1, 4665847.6)	16.6
Pnt 3	(441719.0, 4666022.6)	11.8

3.1.4 Comparison of MPE rainfall with KNMI station data

A comparison was made between the calculated MPE data and the KNMI weather station. The result is shown as Figure 3-2, the maximum derived rainfall rate is 12.8 mm/h which is somewhat less than the observed maximum of 15.7 mm. Also the maximum value's recorded time is one hour earlier than of ground station's recorded time. It is also evident that rainfall derived from satellite tends to underestimate high rain rates as Heinemann et al (2003) cited (Berger, 2003). There may be a number of reasons for this fact. The small extent of the heavy precipitating cells, which is generally below the detection limit of sensors and satellites not passing over the area during the period of the heavy rain are two main reasons for the differences observed.

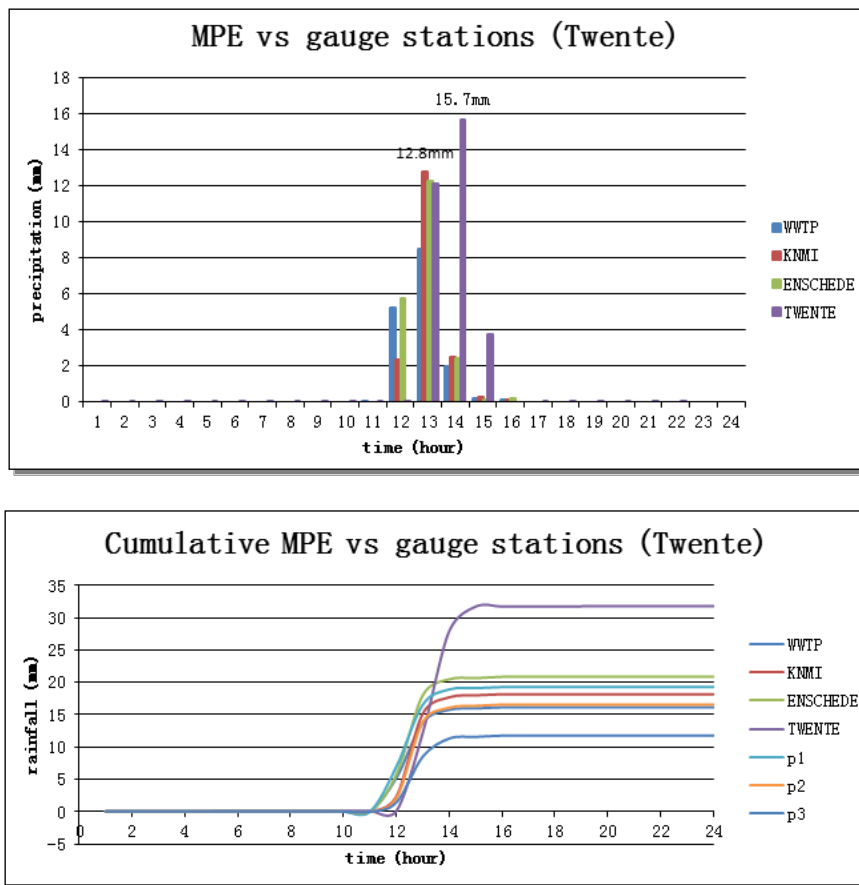


Figure 3-2 Comparison the data of MSG and gauge stations

3.1.5 Conclusion

Referring Figure 3-2 it can be said there is a bias in hourly rainfall values between the MPE data and nearby ground station data under extreme rainfall. Derived rainfall values from satellite is a better option in a situation where there is no short duration weather data. Additionally, the cloud changes dramatically in the convection zone. The following paragraph discuss in details about cloud physical properties.

3.2. Cloud properties under extreme rainfall

3.2.1. Introduction

Clouds play an important role in Earth's water cycle as the intermediate media between the water evaporated from earth's surface and the water returned to the earth by precipitation. Different cloud phase response to several of weather phenomena. Cloud radiative properties in the VIS, NIR and IR wavelengths have been summarized and concluded (Levizzani, 2002).

- Radiative properties in the thermal infrared portion of the electromagnetic spectrum are affected by the size of the hydrometeors. The large particle has a higher transmissivity which increase the emissivity and decrease the reflectivity of the cloud layer.
- The emissivity of water clouds is larger than that of ice clouds
- In the NIR, especially at 3.9 μm clouds with small hydrometeors scatter and reflect more radiance. Big particle size clouds or large drops or ice crystals near the cloud top reduces the 3.9 μm reflectance from the cloud.
- Clouds with ice strongly absorbs the solar radiation in the 3.7-3.9 μm wavelengths.
- NIR reflectance generally relates to the cloud particle effective radius.
- VIS reflectance is mainly related to cloud optical depth.

Numerous instruments and methods have been developed for rain rate retrieval. One of the methods based on geostationary satellites use thermal infrared observations and relate daily minimum cloud top temperature (Anagnostou et al. 1999). This method perform well in convective clouds, but is more weak for higher latitudes (Amorati et al. 2000). Others based on satellite microwave radiometer (MWR) observations like Special Sensor Microwave/Imager (SSM/I). This method use the physical relationship between MWR observed brightness temperatures and columnar water vapor and liquid water path (LWP). The main disadvantage of this method is the low temporal resolution (once a day).

Many researches also show that cloud microphysics can be related to precipitation detection and rain rate. Rosenfeld & Gutman (1994) showed that optically thick cloud with retrieved effective radii larger than 14 μm is required for onset of precipitation. Vicente et al. (1998) developed a technique called auto-estimator (AE), computes rain rates from 10.7 μm brightness temperatures based on a radar-derived rainfall rate estimates and IR cloud-top temperature curve, which is derived from more than 6000 collocated radar and satellite pixels. It is used to produce real-time estimates, average hourly estimates, and 3-, 6-, and 24-h accumulations rain rates. Naus & Kokhanovsky (2007) proposed that cloud liquid water path (LWP) retrieved from Terra-MODIS sensor is directly related to the rainfall probability. Wentz & Spencer (1998) retrieved rain rates from LWP and the height of the rain column. Hence, the liquid water path is an important parameter for clouds. Some researchers also use condense water path (CWP) instead of LWP to make parameterization more general to use (Roebeling & van Meijgaard, 2009). CWP is defined as LWP for water clouds and IWP for ice water path. CWP was computed from cloud optical thickness (COT) and cloud particle effective radius (CRE) (Burrows, et al., 2011). Roebeling & Holleman (2009) developed the Cloud Physical Properties (CPP) algorithm which combines the algorithms mentioned above. It uses information on CWP, CRE and cloud thermodynamic

phase to detect precipitation clouds, CWP and cloud top height (CTH) is used to estimate rain rates.

Thus, good knowledge of the microphysical cloud properties will lead to a better understanding of precipitation, especially for extreme events. In this chapter, we will focus on two algorithms: CPP and AE. The two have the similar spatial and temporal resolution. Data like optimal cloud analysis (OCA), cloud top height (CTH) and cloud top temperature (CTT) retrieved from EUMETSAT for the day of 20th June 2013.

3.2.2. Methods

Assuming a vertically homogeneous cloud, the Cloud Water Path (CWP) was calculated from COT and CRE, more specially, it was calculated from the retrieved COT in the visible (τ_{vis}) at 0.6 μm wavelength and effective drop radius (r_e) of NIR 1.6 μm (Stephens, et al., 1978). Clouds are defined as ice phase if the CTT is lower than 265K. CTT is estimated from the brightness temperature in an infrared window channel (e.g. at 10.8 μm). To derive condensed cloud water path from ice and water phase cloud equation 3-1 is applied.

$$CWP = \frac{2}{3} \tau_{vis} r_e \rho_l \quad [3-1]$$

Where τ_{vis} is COT (dimensionless), r_e is droplet effective radius (μm) and ρ_l is the liquid water density. It can be labelled as precipitating areas when the CWP values are larger than 160g/m², for water clouds, an addition condition is the effective radius (r_e) being smaller than 15 μm (Roebeling et al. 2006).

Once the CWP is achieved, the rain rate (mm/h) can be calculated as

$$R = \frac{c}{H} \left[\frac{CWP - CWP_0}{CWP_0} \right]^\alpha \quad [3-2]$$

Where c and α are constant, CWP_0 is the threshold value for cloud water path (160g/m²) and H is the height of the cloud column. The height if the cloud column is retrieved using following equation.

$$H = \left(\frac{CTT_{max} - CTT_{pix}}{6.5} \right) + dH \quad [3-3]$$

Where CTT_{pix} is the cloud top temperature of current pixel, CTT_{max} is the highest cloud top temperature over an area of the 100×100 pixels. The constant 6.5 is the wet adiabatic lapse rate in K/km. dH is the minimum height of the rain column (0.6km).

Another rainfall equation [3-4] (AE) derived from the relationship between rain rate from weather radar and Infrared brightness temperature (10.7 μm) was used to estimate convective rain rate. In this study SEVIRI 10.8 μm was used.

$$R = 1.1183 \times 10^{11} \exp(-0.036382T_b^{1.2}) a \quad [3-4]$$

Where R is the rain rate in mm/h, T_b is 10.8 μm brightness temperatures in Kelvin.

3.2.3. Data preparation

All the cloud properties data can be ordered by an application published by Eumetsat European Organization after registering and login of their UMARF website (<https://eoportal.eumetsat.int/userMgmt/protected/dataCentre.faces>), a java program which is called EUMETSAT Data Centre Online Ordering (Figure 3-3) can be installed on one's personal computer. Using this program, cloud properties as follow Table 3-3 were downloaded on selected time and format type.

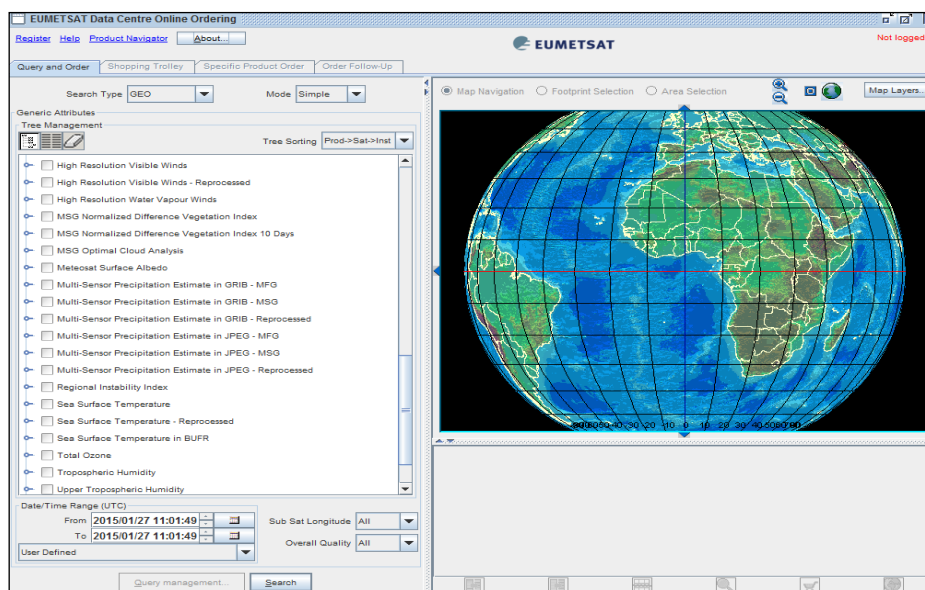


Figure 3-3 MSG data ordering window

Table 3-3 Cloud properties

Name	Data format	Number
Cloud top height (CTH)	GRIB	95
optimal cloud analysis (OCA)	GRIB	24
atmospheric motion vectors (AMV) *	BFR	24
Cloud analysis (CLA) *	BFR	24

*the raw data of AMV and CLA were not processed

3.2.4. Data processing

As listed in the Table 3-3, there are 96 GRIB files on that day at 15 minutes time intervals and 24 BFR files at 1 hour time intervals. These files had to be converted all into ILWIS through DOS based batch processing using the GDAL library or other conversion program, the specific methods was done as following,

For CTH: indicates the height of the highest cloud.

- Using “gdalinfo” under DOS system to view the raw data (Figure 3-4), two bands can be found, band 1 is cloud top height [km], band 2 is cloud top height quality indicator.
- Using “gdal_translate” to translate raw image into Ilwis, for example, under DOS system type the following single command was typed on one line, “gdal_translate -of ilwis input_name.grb output_name”. 95 CTH images were produced in this way in Ilwis.
- Check the image in Ilwis and then make data flag 9999 undefined by an script as “ouput_name:=iff (input_name_band_1 eq 9999,?, input_name_band_1)”. The final map shown as Figure 3-5.

```

C:\Users\apple>cd C:\GDAL\bin
C:\GDAL\bin>gdalinfo MSG3-SEUI-MSGCLTH-0100-0100-20130620001500.000000000Z-1113202.grb
Driver: GRIB/GRIdded Binary (.grb)
Files: MSG3-SEUI-MSGCLTH-0100-0100-20130620001500.000000000Z-1113202.grb
Size is 1237, 1237
Coordinate System is:
PROJCS["unnamed",
  GEOGCS["Coordinate System imported from GRIB file",
    DATUM["unknown",
      SPHEROID["Spheroid imported from GRIB file",6378140,298.252981061491711],
    PRIMEM["Greenwich",0],
    UNIT["degree",0.017453292519943311],
    PROJECTION["Geostationary_Satellite",1],
    PARAMETER["central_meridian",0],
    PARAMETER["satellite_height",35785831],
    PARAMETER["false_easting",0],
    PARAMETER["false_northing",0]],
  ORIGIN = (-5568748.275999999600000,5568748.275999999600000)
Pixel Size = (9003.635046079223700,-9003.635046079223700)
Corner Coordinates:
Upper Left (-5568748.276, 5568748.276) ERROR 1: tolerance condition error
Lower Left (-5568748.276,-5568748.276) ERROR 1: tolerance condition error
Upper Right ( 5568748.276, 5568748.276) ERROR 1: tolerance condition error
Lower Right ( 5568748.276,-5568748.276) ERROR 1: tolerance condition error
Center ( 0.0000000, 0.0000000) ( 0d 0'0.01"E, 0d 0'0.01"N)
Band 1 Block=1237x1 Type=Float64, ColorInterp=Undefined
  Description = 0.000[-] undefined (<)
  Metadata:
    GRIB_UNIT=[kg/(m^2*s)]
    GRIB_COMMENT=Cloud top height [kg/(m^2*s)]
    GRIB_ELEMENT=
    GRIB_SHORT_NAME=0 undefined
    GRIB_REF_TIME= 1371687300 sec UTC
    GRIB_VALID_TIME= 1371687300 sec UTC
    GRIB_FORECAST_SECONDS=0 sec
    GRIB_PDS_PDIN=30
    GRIB_PDS_TEMPLATE_NUMBERS=1 2 8 3 1 1 77 0 57 207 255 255 255 255 255
Band 2 Block=1237x1 Type=Float64, ColorInterp=Undefined
  Description = 0.000[-] undefined (<)
  Metadata:
    GRIB_UNIT=[(0 Nominal cloud top height quality, 1 Fog in segment, 2 Poor quality height estimation)3 Fog in segment and poor quality height estimation]
    GRIB_COMMENT=Cloud top height quality indicator [(0 Nominal cloud top height quality, 1 Fog in segment, 2 Poor quality height estimation)3 Fog in segment and poor quality height estimation]
    GRIB_ELEMENT=
    GRIB_SHORT_NAME=0 undefined
    GRIB_REF_TIME= 1371687300 sec UTC
    GRIB_VALID_TIME= 1371687300 sec UTC
    GRIB_FORECAST_SECONDS=0 sec
    
```

Figure 3-4 Example of using “gdalinfo” to check CTH data

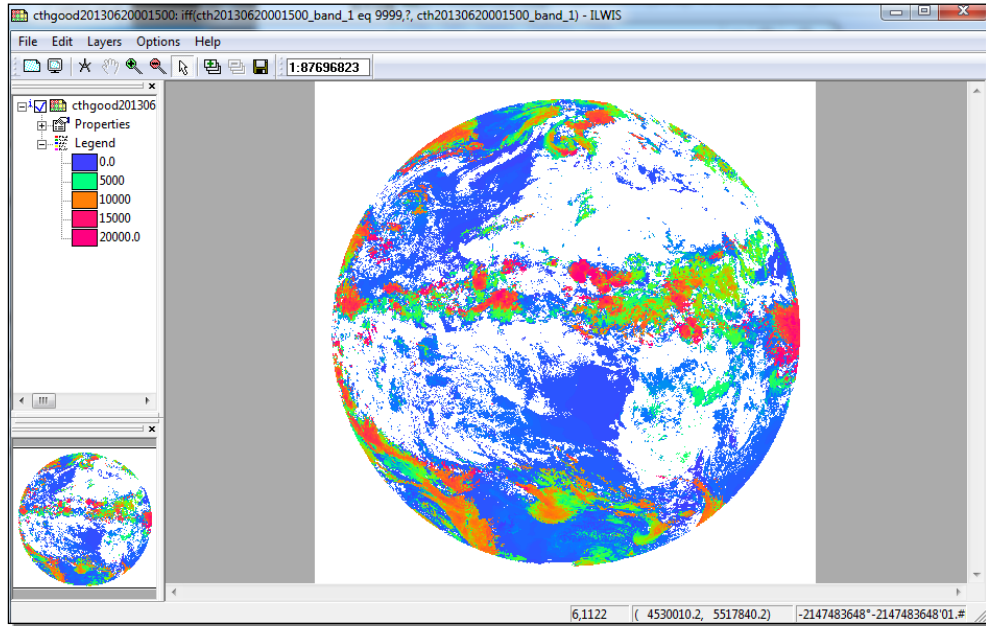


Figure 3-5 Example of processed CTH image on June 20th 2013

For OCA: The Optimal Cloud Analysis is an algorithm to extract the principal cloud parameters like cloud phase, cloud top pressure (CTP), cloud optical thickness(COT) and cloud effective radius(CRE) using an optimal estimation method and simultaneously all the SEVIRI spectral measurements (EUMETSAT, 2010).

- Using “gdalinfo” under DOS system to see the raw data (Figure 3-6), 12 bands can be found. Table 3-4 was used to encode these 12 bands. It shows the parameter numbers response for different bands, band (2-12) response for Number (24-34).
- The same script used in CTH above is also used here to transform raw data under DOS system and replace the undefined value. 24 images of each parameter (Figure 3-7) were processed and used in further study.

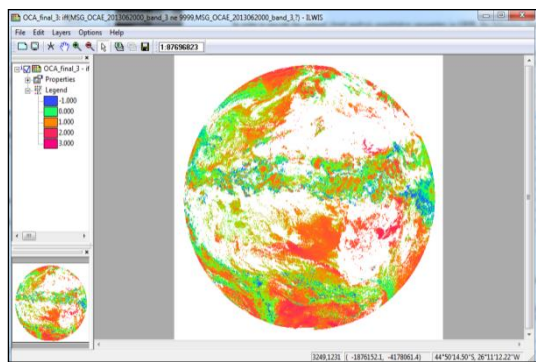
```

C:\GDAL\bin>GDALINFO MSG3-SEUI-MSGOCAE-0100-0100-20130620000000.000000000Z-11098
22.grb
Driver: GRIB/Gridded Binary (.grb)
Files: MSG3-SEUI-MSGOCAE-0100-0100-20130620000000.000000000Z-1109892.grb
Size is 3712, 3712
Coordinate System is:
PROJCS["unnamed",
  GEOGCS["Coordinate System imported from GRIB file",
    DATUM["unknown"],
    SPHEROID["Spheroid imported from GRIB file",6378140.298,252981061491
711],
    PRIMEM["Greenwich",0],
    UNIT["degree",0.01745329251994331],
    PROJECTION["Geostationary_Satellite"],
    PARAMETER["central_meridian",0],
    PARAMETER["satellite_height",35785831],
    PARAMETER["false_easting",0],
    PARAMETER["false_northing",0]]
Origin = (-5568748.275999999600000,5568748.275999999600000)
Pixel Size = (3000.403165948275700,-3000.403165948275700)
Corner Coordinates:
Upper Left (-5568748.276, 5568748.276) ERROR 1: tolerance condition error
Lower Left (-5568748.276, -5568748.276) ERROR 1: tolerance condition error
Upper Right ( 5568748.276, 5568748.276) ERROR 1: tolerance condition error
Lower Right ( 5568748.276, -5568748.276) ERROR 1: tolerance condition error
Center ( 0.0000000, 0.0000000) ( 0d 0'0.01"E, 0d 0'0.01"N)
Band 1 Block=3712x1 Type=Float64, ColorInterp=Undefined
Description = 0.000[-] undefined (<)
Metadata:
  GRIB_UNIT=[0 No scene, 1 needle, 2 broad-leafed, 3 Deciduous needle, 4 Deci
duous broad-leafed, 5 Deciduous mixed, 6 Closed shrub, 7 Open shrub, 8 Woody sav
annah, 9 Savannah, 10 Grassland, 11 wetland, 12 Cropland, 13 Urban, 14 crops, 15
snow, 16 Desert, 17 Water, 18 Tundra, 97 Snow on land, 98 Snow on water, 99 Sun
-glint, 100 General cloud, 101 (fog, Stratus), 102 Stratocumulus, 103 Low cloud,
104 Nimbostratus, 105 Altostratus, 106 Medium cloud, 107 Cumulus, 108 Cirrus, 10
9 High cloud, 110 Unknown cloud]
  GRIB_COMMENT=[Pixel scene type [0 No scene, 2 broad-leafed, 3 Deci
duous needle, 4 Deciduous broad-leafed, 5 Deciduous mixed, 6 Closed shrub, 7 Ope
n shrub, 8 Woody savannah, 9 Savannah, 10 Grassland, 11 wetland, 12 Cropland, 13
Urban, 14 crops, 15 snow, 16 Desert, 17 Water, 18 Tundra, 97 Snow on land, 98 S
now on water, 99 Sun-glint, 100 General cloud, 101 (fog, Stratus), 102 Stratocum
ulus, 103 Low cloud, 104 Nimbostratus, 105 Altostratus, 106 Medium cloud, 107 Cum
ulus, 108 Cirrus, 109 High cloud, 110 Unknown cloud]]
  GRIB_ELEMENT=
  GRIB_SHORT_NAME=0 undefined
  GRIB_REF_TIME= 1371686400 sec UTC
  GRIB_VALID_TIME= 1371686400 sec UTC
  GRIB_FORECAST_SECONDS=0 sec
  GRIB_PDS_PDTM=30
  GRIB_PDS_TEMPLATE_NUMBERS=0 8 8 8 1 1 77 0 57 207 255 255 255 255 255
Band 2 Block=3712x1 Type=Float64, ColorInterp=Undefined
Description = 0.000[-] undefined (<)
Metadata:
  GRIB_UNIT=[-]
  
```

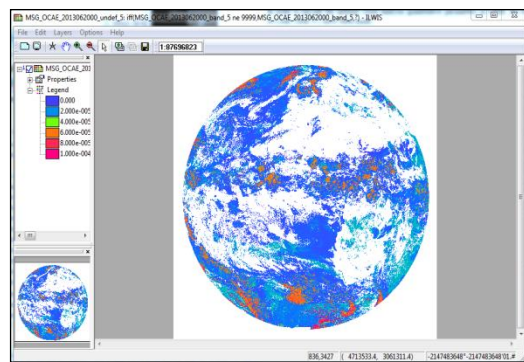
Figure 3-6 Example of using “gdalinfo” to check OCA raw data

Table 3-4 OCA parameters

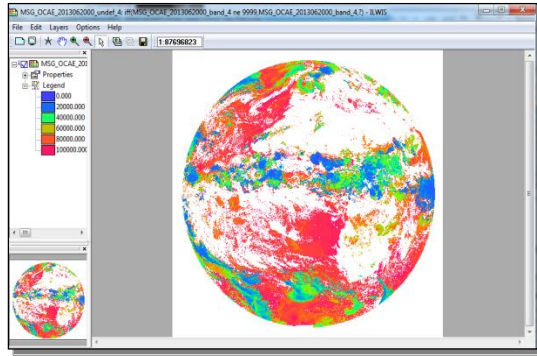
Number	Parameter Name	Units	Abbrev
24	Measurement Cost	-	JM
25	Upper Layer Cloud Optical Thickness	-	ULCOT
26	Upper Layer Cloud Top Pressure	Pa	ULCTP
27	Upper Layer Cloud Effective Radius	m	ULCRE
28	Error in Upper Layer Cloud Optical Thickness	-	ERR-ULCOT
29	Error in Upper Layer Cloud Top Pressure	Pa	ERR-ULCTP
30	Error in Upper Layer Cloud Effective Radius	m	ERR-ULCRE
31	Lower Layer Cloud Optical Thickness	-	LLCOT
32	Lower Layer Cloud Top Pressure	Pa	LLCTP
33	Error in Lower Layer Cloud Optical Thickness	-	ERR-LLCOT
34	Error in Lower Layer Cloud Top Pressure	Pa	ERR-LLCTP
35 - 191	Reserved	-	-



COT



CER



CTP

Figure 3-7 Example of processed OCA image on June 20th 2013

For CTT: indicates cloud top temperature (K).

- This was retrieved from thermal SERIVI channel (IR_108) HRIT file through MSG Data Retriever in GEONETCast as Figure 3-8.

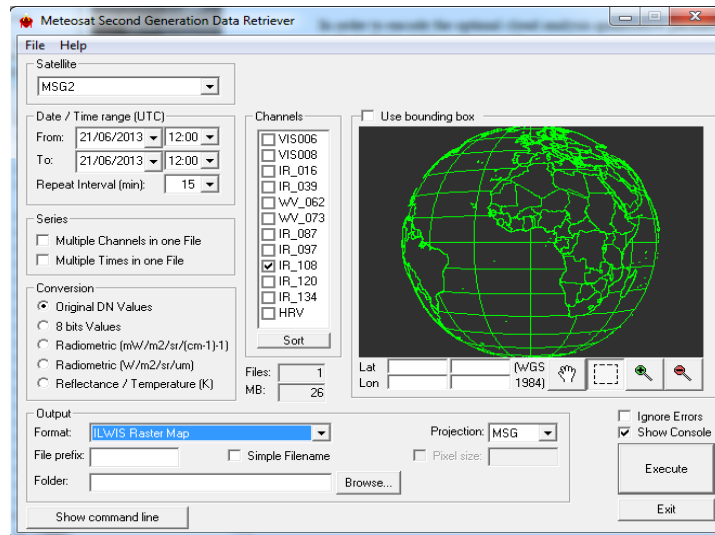


Figure 3-8 Example of using MSG Data Retriever to get CTT value

3.2.5. Data extraction

All the cloud properties images (ILWIS map files) were resampled to the Twente region, the method of nearest neighbor were used for resampling. Then 3 points defined in the previous were chosen considering the position of the sub-catchment. An ILWIS script function has been made and used to extract data from an image stack that contains 95 layers of CTH, 96 layers of CTT and 24 layers of OCA data (COT, CRE). This data set was used in the analysis of following section.

3.2.6. Data analysis

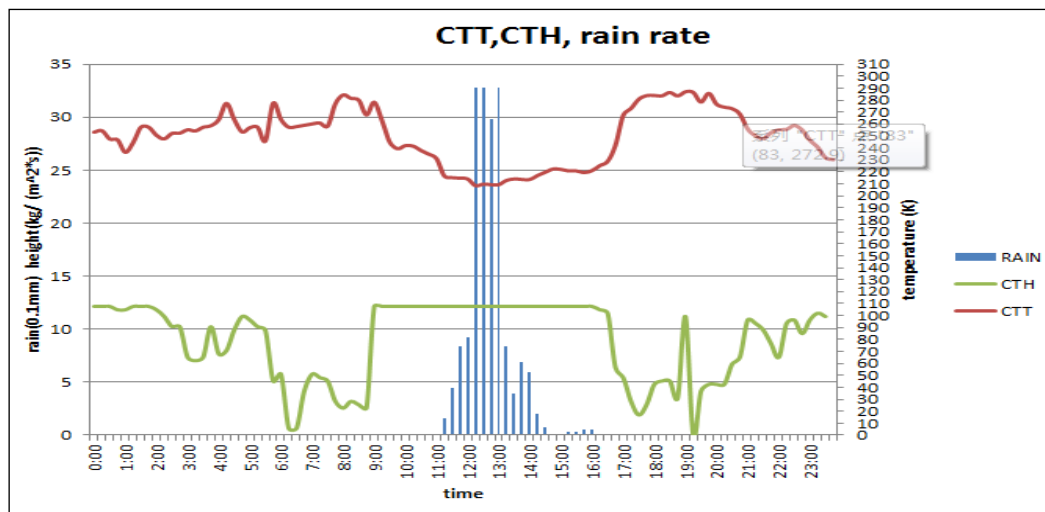


Figure 3-9 Comparison between CTT and CTH

A comparison was made among rain rate, CTT and CTH, the results are presented in the Figure 3-9. It shows an opposite trend between CTH and CTT, the value was changed dramatically after 9:00 which is almost two hour before precipitation occurred. During rainfall, the average CTT and CTH is 217K and 12.16 km respectively, but CTH presented as a straight line may be due to sensor error. The observed value is generally beyond the detection limit of satellite sensors. To calibrate this value, equation 3-5 was adopted as following.

$$CTH = \left(\frac{T_{surf} - CTT}{5.5} \right) \quad 3-5$$

Where T_{surf} is the surface temperature (use of a daily average rainfall for Twente), CTT is the cloud top temperature computed in the CPP algorithm and 5.5 K/km is the moist adiabatic lapse rate. By doing such correction, the values were calibrated and shown in Figure 3-10.

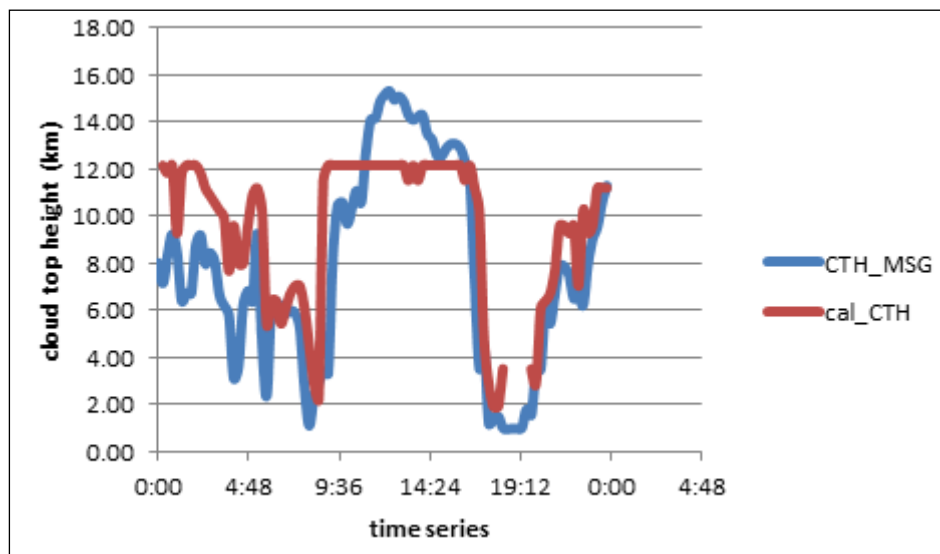


Figure 3-10 Comparison of CTH retrieved from MSG and calibrated CTH using equation 3-5.

To determine the optimum setting of the CPP and AE algorithm, the SEVIRI retrievals of rain rates and the experimental derived rain rates are compared against the rain gauge observations. The comparison is done for an independent calibration data set obtained between 13:00 and 15:00 UTC on 20th June 2013. The optimum settings found for the retrieval of rain rates for CPP are: CTH = H and $\alpha=1.6$ and $c=40$.

The results of the day two algorithms in detection and retrieval of rain rate for Twente region are given. Since the CPP retrievals are limited to daylight hours (solar zenith angles $< 72^\circ$), time for the date (20130620) of the event were restricted to between 10:00 UTC and 17:00 UTC at 1 hour time step.

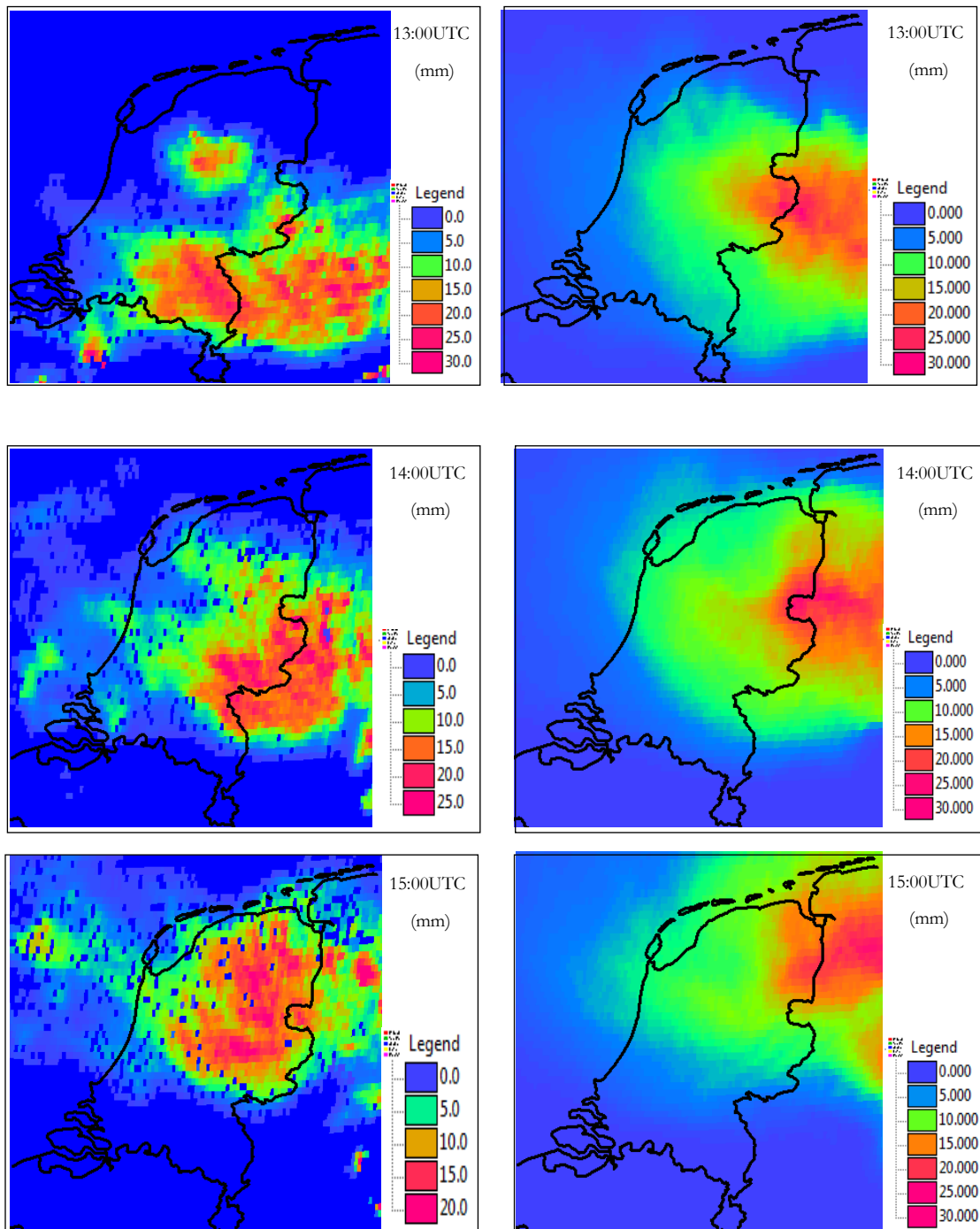


Figure 3-11 Rainfall (mm/h) derived from CPP (left) and AE (right) algorithms on 20th June 2013, 13:00-15:00 UTC

Roebeling et al. (2012) mentioned, the precipitation in the summer time over land are dominated by convective clouds and the strongest convection is typically found in the afternoon. This was explained as being that the daylight-only diurnal cycle of land surface temperature and the convective cloud systems activated with the heated surface during the day and collapses with the cool surface during the night. The duration of the extreme events over Twente region was just start from 13:00 UTC to 15:00 UTC. Figure 3-12 displays the rainfall map from two algorithms, which show the similar movement path of precipitation clouds. CPP (left) provides the distribution of rain rate in a little more detail, while AE (right) gives a relative wide range of rainfall area as its high response to the CTT. In order to exclude unrealistically high rain rates, the estimates are limited to a maximum intensity of 40 mm/h.

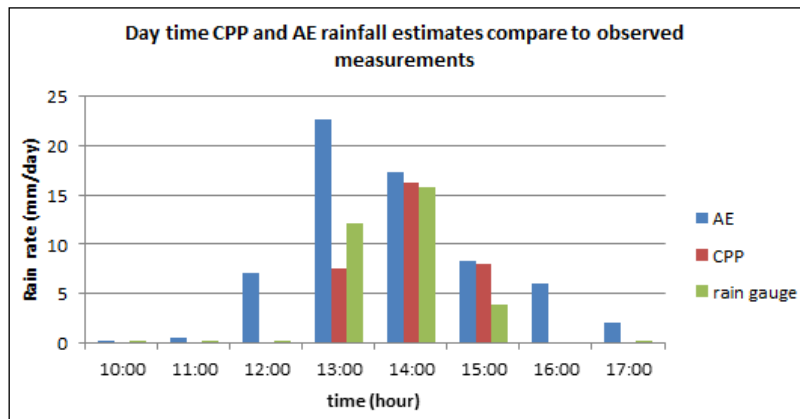


Figure 3-12 CPP and AE compared to observed rain gauge measurements on 20th June 2013

Table 3-5 Statistical analysis of results on 20th June between the algorithms of the day's total estimates

	Obs/AE	Obs/ CPP
Total rain rate	62.964	31.7
Mean Bias	4.037	0.003
RMSE	0.809	0.90
Correlation	0.706	0.91

The CPP and AE day total rainfall estimates were compared with rain gauge measurements at Twente station. Table 3-5 showing the categorical analysis results of each algorithm in relation to observed value. Line plot were also used to describe the relationship between CPP and AE. Good correlation and reasonable Root Mean Square Error (RMSE) are observed from CPP, while AE gives an overestimated peak value and extended precipitation duration corresponding to the same events. It may be caused by the slow moving and large cold-topped clouds.

3.2.7. Discussion

These two precipitation estimates method are used to produce real-time estimates and show better results for heavy rainfall systems. AE algorithm gives a rapidly and operational way to

separate the delineation of precipitating clouds which had a 250K for non-convective rain rate and 240K for convective rain rate (Scofield & Kuligowski, 2003). This method also can be applied at night. However, since it is an experimental equation, it highly depends on large amount of radar and/or rain gauge data to calibrate. CPP algorithm in retrieval of rain rate from IR instruments also performs well, and it has been very reliable for the assessment of precipitation areas (Beaumont et al.2013). Due to its combination of information on CWP with that on cloud top microphysical properties, the accuracy is obviously improved. However, poor performance in winter, at night or in lower zenith angle area is a big issue in its application. Maybe combination of CPP and AE can be a compromised way to solve this problem.

3.3. Regional occurrence of extreme rainfall

Regional heavy rainfall events can trigger disasters for human beings, such as urban flooding can cause severe damage to lives and property. An essential concern is what the behaviour of the extreme events occurrence frequency is.

One of method to solve this question is the precipitation percentile. It can be defined as, the nth percentile of an observation variable which is the value that cuts off the first n percent of the data values when it is sorted in ascending order. A threshold should be chosen first to define extreme rainfall; usually we choose 99th percentiles (R99T) as heavy rain and 99.9th percentiles (R99.9T) as extreme events (Groisman et al., 2005).

There are over 40 years daily data (1974 to 2014) in Twente area provided from KNMI. Data processing can be described as follows,

- Negative value means rainfall lower than 0.05mm, replace them with zero
- Filter the value which is greater than 0.1mm/day and sort it in ascending order
- Use the function to get 99th percentiles in Excel

The result showed that $R99T = 25\text{mm/day}$ and $R99.9T = 43.6\text{mm/day}$, Figure 3-13 was created to show how many times daily rainfall larger than R99T and R99.9T in every year, than return period of extreme rainfall was calculated as 4.3 years, and annual exceedance probability of a extreme event over 43.6 mm/day $= 43.6/4.3 = 10.2\%$. After listing the maximum daily data in every year in Figure 3-14, it was found out that rain rate became unstable. The maximum value was 6 times more than minimum value. Also from the Table 3-6, almost 8% max daily rainfall is extreme rainfall event.

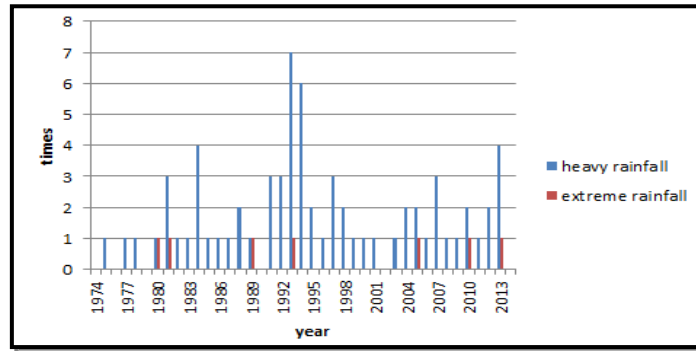


Figure 3-13 Times of rainfall larger than R99T (heavy rainfall) and R99.9T (extreme rainfall)

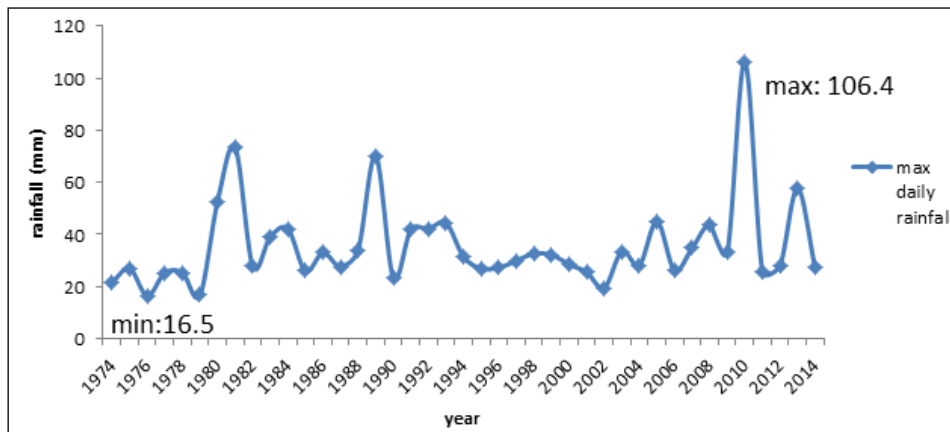


Figure 3-14 Max daily rainfall in every year

	1970	1980	1990	2000	2010	
0		52.7	23.3	28.6	106.4	3
1		73.5	41.9	25.5	25.7	3
2		27.9	42.2	19.5	27.9	
3		39.1	44.4	33.5	57.8	
4	21.7	42.2	31.5	28.3	27.2	
5	27	26	26.9	45		
6	16.5	33	27.3	26.3		
7	25.3	27.6	29.9	34.8		3
8	25.3	34	32.7	43.6		
9	16.7	70.3	32.2	33.3		

Between 1974 and 2014: 8 events 7 intervals, ranging from 1 to 11 years

Figure 3-15 Frequency analysis

class interval(mm)	times	relative frequency(%)
<25	5	12
25-43.6	28	68
>43.6	8	20

Table 3-6 Relative frequency of heavy rainfall and extreme rainfall

4. DEM DATA PROCESS AND ANALYSIS

In order to perform rainfall – runoff modeling a multitude of geographic information is needed. The input data of model can be provided through processing and analysis of Digital Elevation Models (DEM).

This chapter compares different DEM resolutions for delineation and draining network extraction in urban and semi-urban areas. Since the elevation in Enschede higher then Hengelo, we choose Enschede area as selected model area for DEM hydro-processing, and more specially the drainage area of the Kristalbad (i.e.”Elsbeek”).

4.1. Two resources of near global elevation data sets

4.1.1. Shuttle Radar Topographic Mission (SRTM) based DEM

In this case, SRTM 1 Arc-Second Global elevation data were selected and the data information listed in Table 4-1. These data would be used by spatial application software as input data.

Table 4-1 SRTM data format

Data Set Attribute	Attribute Value
Entity ID	SRTM1N52E006V3
Horizontal Datum	WGS84
C-band Wavelength	5.6 cm
Format	TIFF
Lat/Long	52.22N 6.89E
Spatial Resolution	30 meters
Units	Meters
Pixel Depth	16 Bit

4.1.2. Actual Height Netherlands (AHN) based DEM

On the download website (PDOK), there are two kinds of datasets (AHN1, AHN2).

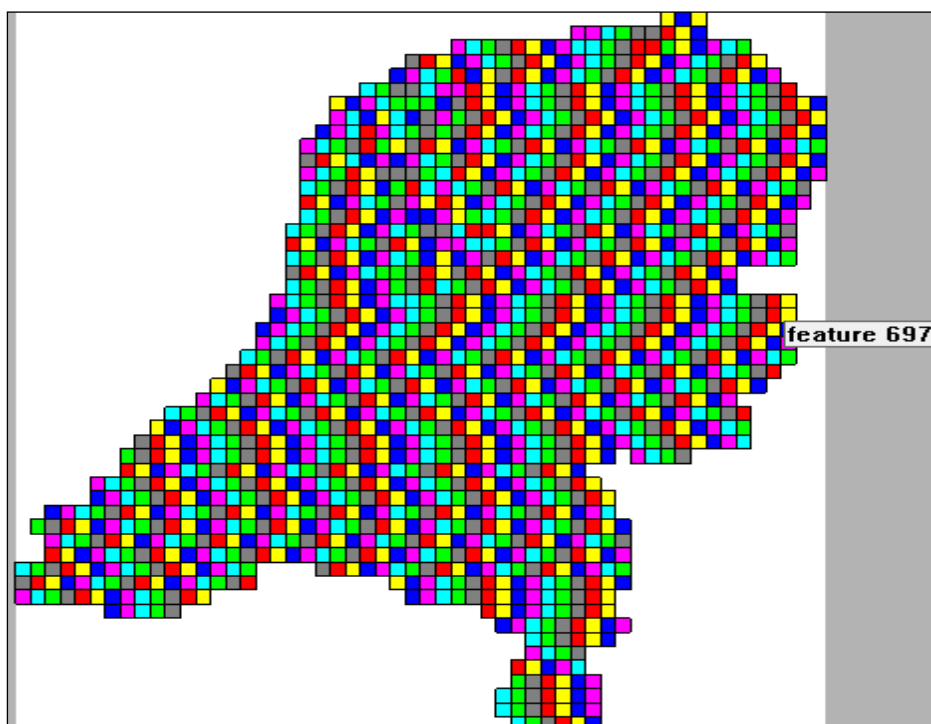
AHN1: ground level dataset, no buildings and trees information in the rural area

AHN2: ground data with all vegetation and buildings information

The resolution for AHN1 is from 5 to 100 meters and for AHN2 from 0.5 to 5 meters. In this case, 5 and 0.5 meters raster data of each kind were used. Since the download link is in GML format, many necessary processes need to be performed as follows,

- An AHN-units map (Figure 4-1) was downloaded and imported using ILWIS 3.84.
- Find the area of interest and read the related feature number from the AHN-units map.
- Open the table of AHN-units map in ILWIS and search the tile name response to the feature number from UNIT column.
- Go back to the XML file and use the tile name to get the download address.

Figure 4-1 AHN-units map display by ILWIS



After using this method, three raster maps (34fn1, 34fn2 and 35an1.tiff) were downloaded. To make the further process easily, these maps can be merged into a single map by using ILWIS – Raster Operation – Glue Maps. Some basic information on the DEM is listed as Table 4-2.

Table 4-2 AHN data format

Data Set Attribute	Attribute Value
Spatial resolution	AHN1: 5 m
	AHN2: 0.5m
Coordinate system	Amersfoort RD New
Linear Unit	1 cm height
Format	TIFF
Pixel Depth	32 Bit

4.2. Data processing

The DEM hydro-processing was performed using the functions of the ILWIS-GIS package (Maathuis & Wang, 2006) developed at ITC. Many approaches have been incorporated within the package can help the user to derive a realistic river and basin schematization. A schematization of the processes is shown in the Figure 4-2. Ultimately, the main catchment, sub-catchments based on the stream intersection points and drainage paths were extracted.

Schematic overview drainage and catchment parameter extraction

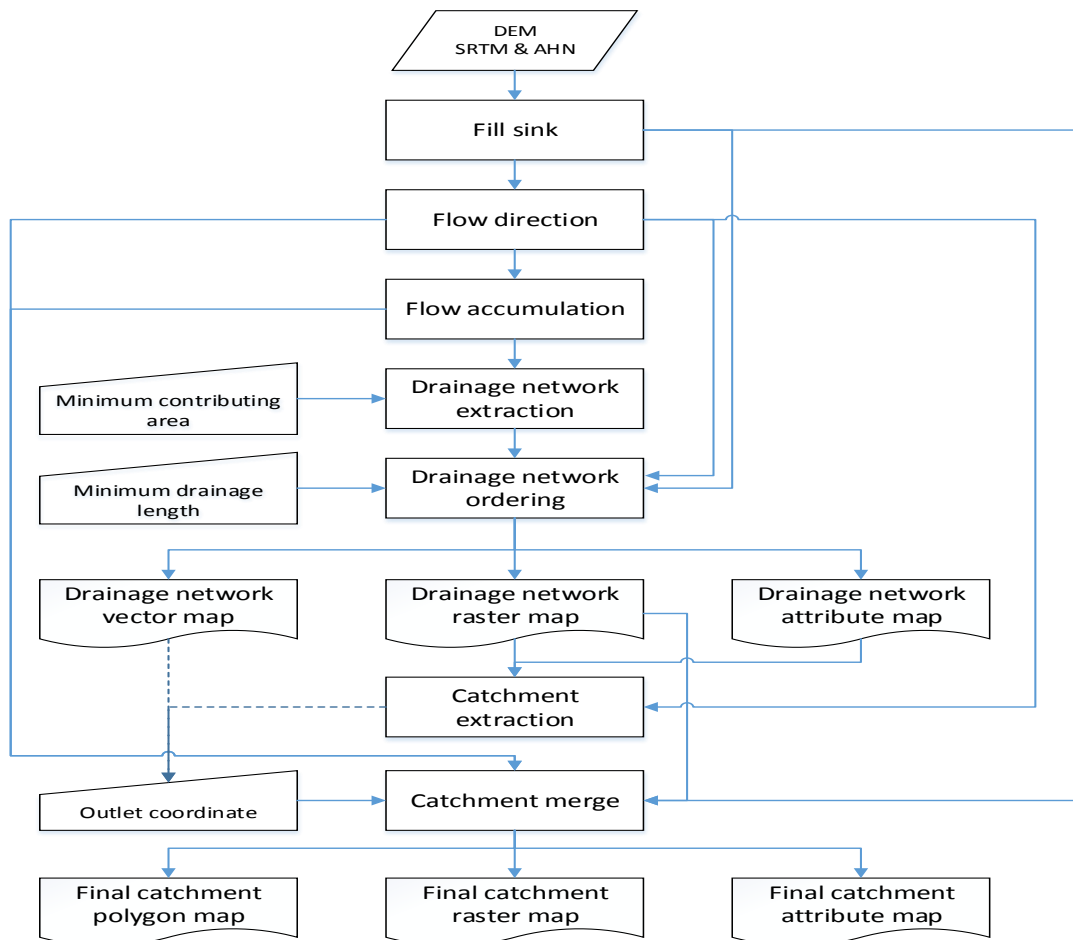


Figure 4-2 DEM hydro-processing procedure for drainage network and sub-catchment extraction

The final resulting sub-catchment maps from different sources and resolutions are shown as Figure 4-3 and 4-4. It is an essential output of the DEM hydro-process so as to obtain the land use and land cover (LULC) data.

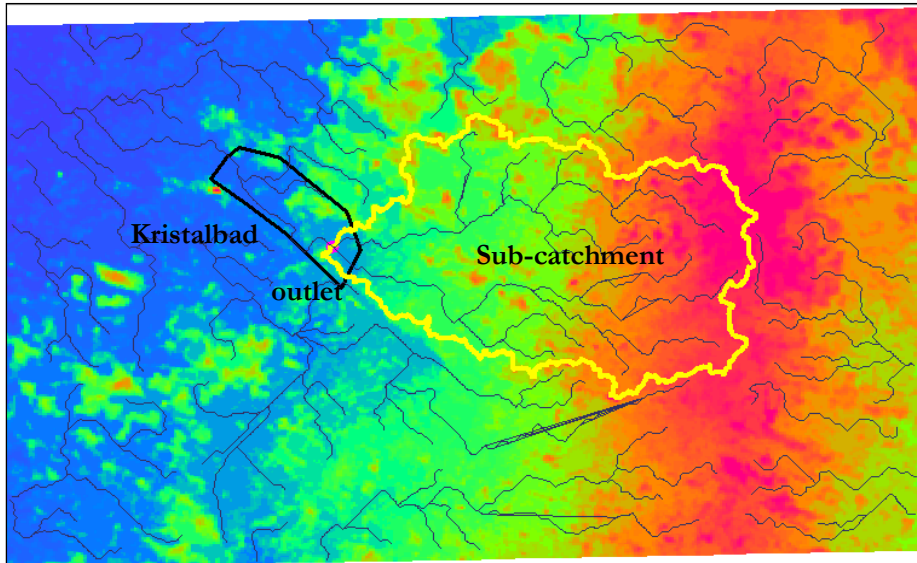


Figure 4-3 Sub-catchment for SRTM based DEM (spatial resolution: 30m)

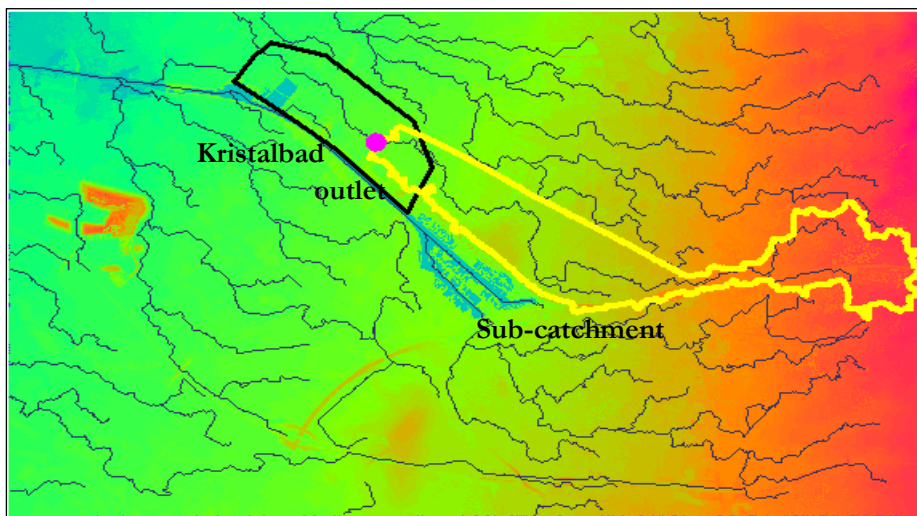
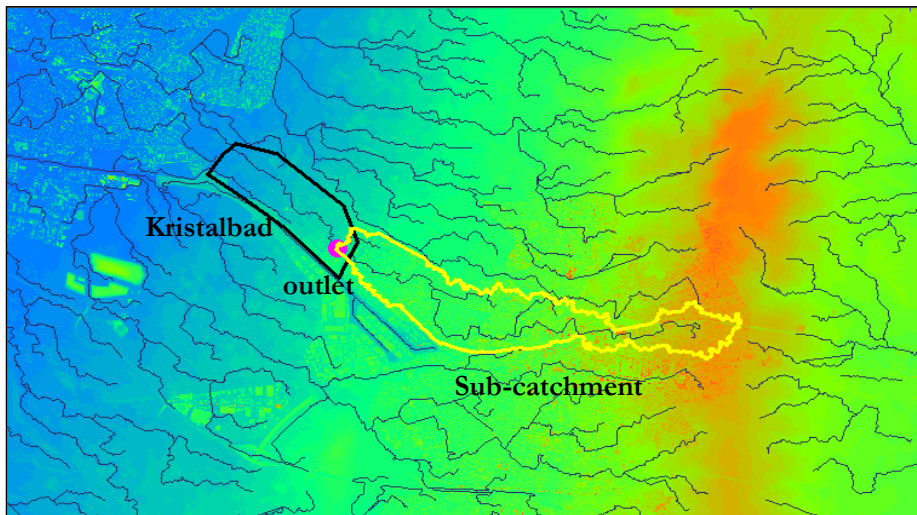


Figure 4-4 Sub-catchment for AHN based DEM (spatial resolution: 5m and 0.5m respectively)

Table 4-3 Sub-catchment properties from each DEM

Field name	Catchment area (m ²)	Drainage density (m/km ²)	Upstream max elevation (m)	Outlet elevation (m)
SRTM (30m)	16527337.50	2135.01	64.00	26.00
AHN (5m)	4120012.50	3138.19	57.53	26.93
AHN (0.5m)	4404475.00	2813.00	56.00	27.00

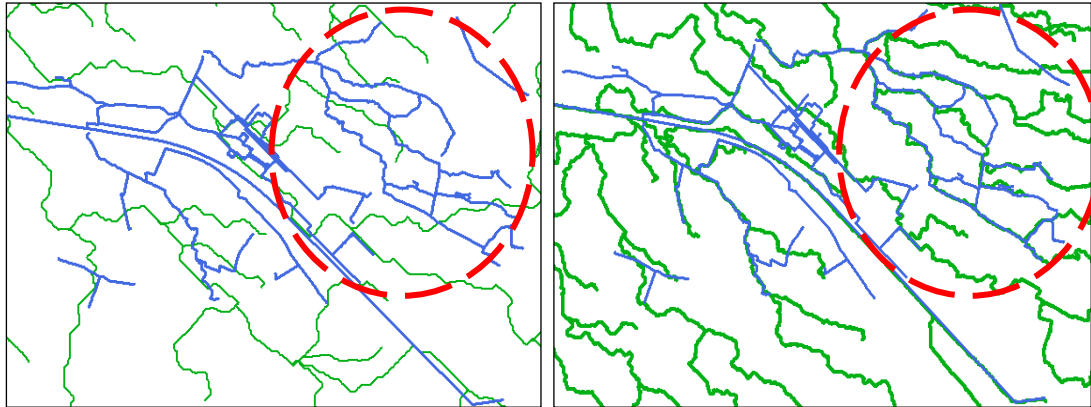


Figure 4-5 SRTM (30m) based drainage network (left) compared with AHN (5m) based drainage network

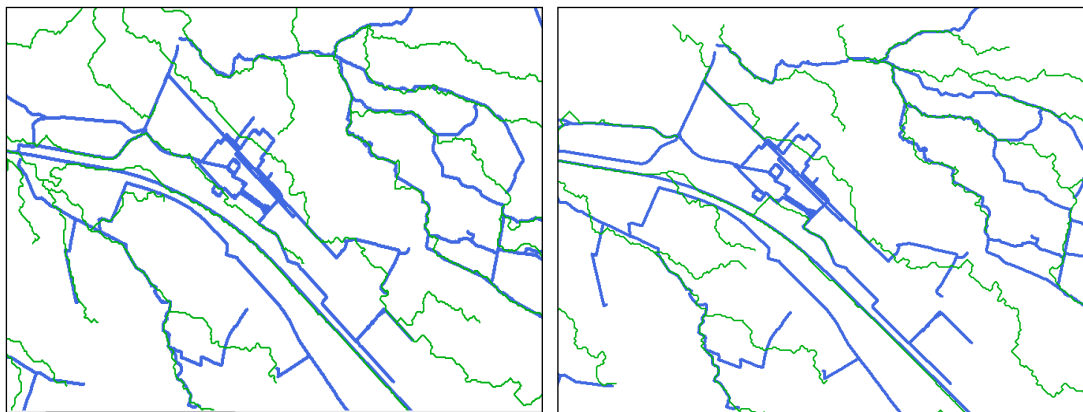


Figure 4-6 AHN 5m (left) vs. 0.5m (right) resolution based drainage network

A comparison was made to select the best fit drainage network used to merge sub-catchments. The real network around Kristalbad is shown in blue line. Quite a large area of sub-catchment (Figure 4-3) gotten from SRTM (30m), but the drainage network (Figure 4-5, left) shows a poor fitness compared to the real one. Two long and narrow sub-catchments (Figure 4-4) were created from AHN 5m and 0.5m resolutions. The drainage network (Figure 4-6) for this data source shows a relatively good agreement when linked with the real network. Especially for 0.5m resolution, it can be found that the channel from WWTP to Kristalbad matched perfectly. Thus, the land cover and land use map (LULC) retrieved from AHN 0.5 m was used as the collecting area after rainfall events and was further used in the Duflow model.

4.3. LULC reclassification

Land cover-land use (LULC) data is fundamental information required in hydraulic modeling. In this study, only three main classes are of interests: open water, paved surface and unpaved surface, and each category in percentages was used as input for modeling.

The outline map was provided from previous work from AHN 0.5m map and the TOP10NL map used as the background of topographic features. TOP10NL is the digital topographic base file from the Dutch Land Registry. It is the most detailed product within the Register Topography. It is nationwide and in this study the map of Netherlands can be downloaded from PDOK.

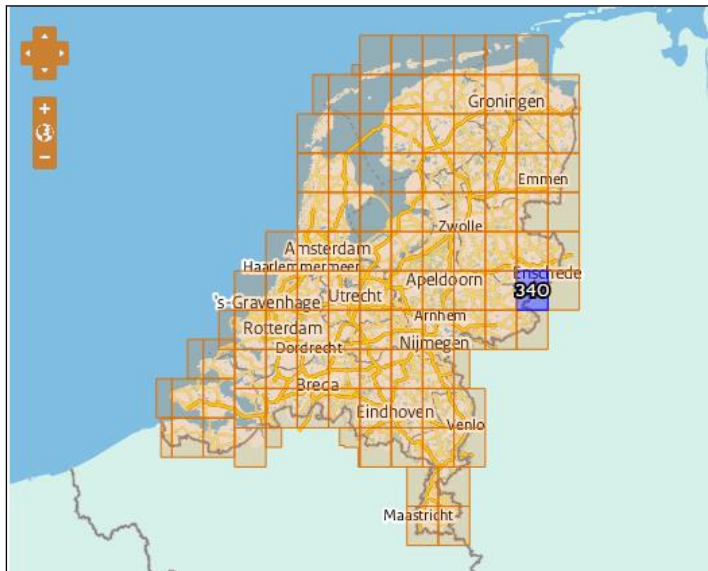


Figure 4-7 Example of TOP10NL map download from PDOK, layout scale 1:50,000

The code “340” was selected in GML format from the website as it completely covers the study area. All the processing was done in the ArcGIS environment. The outline of the sub-catchment map was first rasterized to polygon map and intersected with the TOP10NL_340 (Figure 4-8).

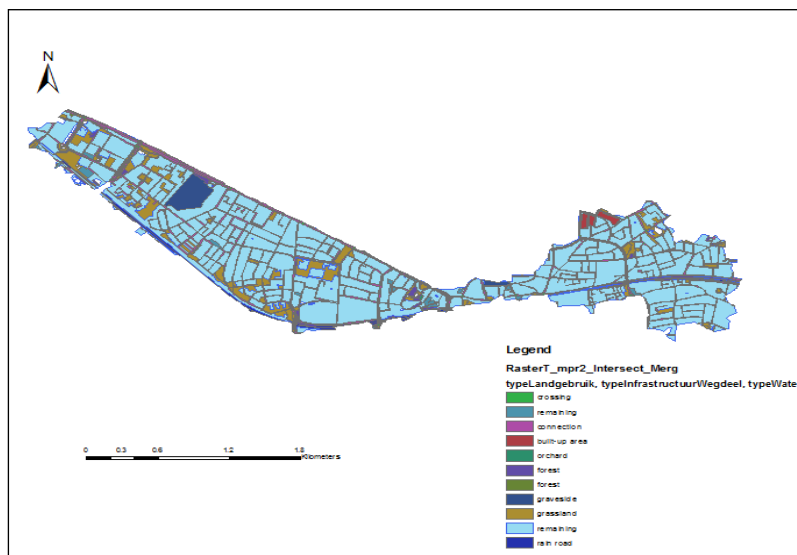


Figure 4-8 LULC map extract from TOP10NL

Table 4-4 Reclassifications of land cover classes for modeling

	Land cover	Reclassification
1	Forest	Unpaved
2	Railway section	Paved
3	Remaining	Paved
4	Road section	Paved
5	Water portion	Open water
6	Build-up area	Paved
7	Orchard	Unpaved
8	Graveside	Paved
9	Grassland	Unpaved

The land cover classes had been re-categorized as presented in the Table 4-4. All categories were selected by attribute and labelled in the new classes, then by using the dissolve operation the reclassification map (Figure 4-9) was generated in ArcGIS software.

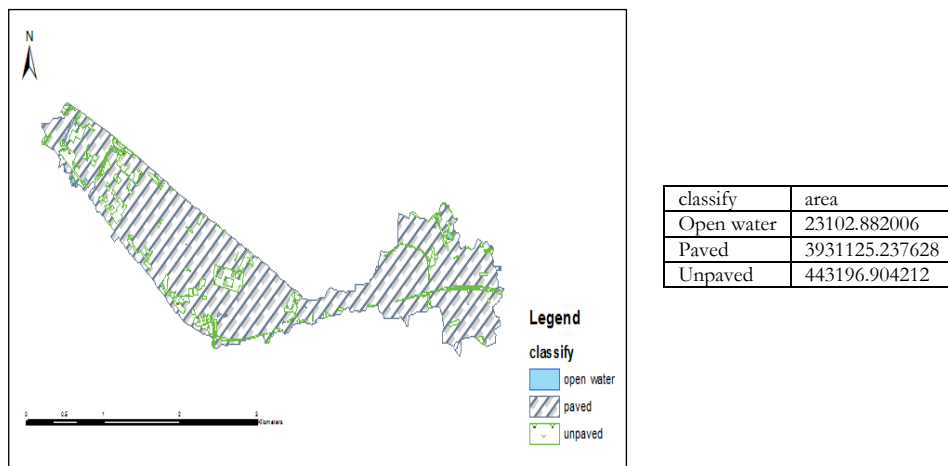


Figure 4-9 Reclassification map and properties of the sub-catchment

5. HYDRODYNAMIC MODELING

5.1. Duflow Modeling Studio (DMS)

Duflow is a flexible computer software for simulating one-dimensional water movement and water quality package for steady, unsteady flows in networks of canals, rivers and channels. It is a public – domain software and can be acquired at a nominal cost (Clemmens et al., 1993). It supports the dynamic management of water systems in many areas, such as for industry, agriculture, domestic supply, flood and water quality control (DUFLOW, 2004). The program provides the modeler a user-friendly graphical user interface (GUI). In this environment, model data can be entered easily; with the Network Editor, a network can be built by dragging and clicking of objects. This program is commonly used by the water authorities, related infrastructure designer and for education/research purposes.

The DMS program is designed for simple networks of channels with simple structures. The Duflow Modeling Studio contains the following key features;

- Duflow water quantity
Used for steady and unsteady flow computations in networks of open water courses
- Duflow water quality
Simulate the transportation of substances in free surface flow and other complex water quality processes.
- RAM precipitation runoff module
Calculate the supply of rainfall to the surface flow and modeling rainfall runoff processes from land areas.
- MODUFLOW
Simulate integrated ground water and surface water problem by combining the Duflow with MODUFLOW.

5.2. Duflow model

DUFLOW simulation is based on the one-dimensional partial differential equations that describe non- stationary flow in open channels. These equations, which are the mathematical translations of the laws of conservation of mass and momentum:

$$\frac{\partial B}{\partial t} + \frac{\partial Q}{\partial x} = 0 \quad \text{5-1 Continuity equation}$$

$$\frac{\partial Q}{\partial t} + gA \frac{\partial H}{\partial x} + \frac{\partial(\alpha Qv)}{\partial x} + \frac{g|Q|Q}{C^2 AR} = a\gamma w^2 \cos(\Phi - \phi) \quad \text{5-2 Momentum equation}$$

Where:

B(x, H)	cross-sectional storage area [m ²]
Q(x, t)	discharge at location x and at time t [m ³ /s] Q=VA
t	time [s]

x	distance as measured along the channel axis [m]
$H(x, t)$	water level with respect to reference level [m]
$\Lambda(x, H)$	cross-sectional area [m ²]
g	acceleration due to gravity [m/s ²]
$v(x, t)$	mean velocity (averaged over the cross-sectional area) [m/s]
$R(x, H)$	hydraulic radius of cross-section [m]
$a(x, H)$	cross-sectional width [m]
$b(x, H)$	cross-sectional storage width [m]
α	correction factor for non-uniformity of the velocity distribution in the advection term
$C(x, H)$	coefficient of De Chézy [m ^{1/2} /s]
$w(t)$	wind velocity [m/s]
$\Phi(t)$	wind direction in degrees
$f(x)$	direction of channel axis in degrees, measured clockwise from the north
$\gamma(x)$	wind conversion coefficient [-]

The mass equation [5-1] states that the water level changes is equal to inflow minus outflow at some location. The momentum equation [5-2] expressed that the momentum changes affect by interior and exterior forces like friction, wind and gravity. After solving the above equations [5-1,5-2], each channel will have unknown discharges (Q) and heads (H) in two equations for new time level (Subramanya, 2009). For the derivation of these equations it has been assumed that the fluid is well mixed and the density is constant.

To get the unique solution of the set of equations additional conditions have to be determined at boundaries of the network and at the sections defined as hydraulic structure. These user-defined conditions at the physical boundaries can be levels (H), discharges (Q) or a QH relation.

5.3. Duflow rainfall runoff (RAM) component

The precipitation runoff model describes the process in the hydrological cycle that water from the rainfall gets to be the discharged as a result of run off to the ground water or surface water. This process is commonly used at a catchment area level since the relevant parameters may vary substantially. In this research, the essential input parameters were the terrain properties of catchment, soil information, precipitation and evaporation data.

In RAM, the linear reservoir model is applied to describe the rainfall runoff processes. The effective precipitation as input in these models and also the diversity of surface types link to the different precipitation runoff processes. The framework of the precipitation runoff module from the Duflow manual (DUFLOW-RAM, 2004) is shown in Figure 5-1.

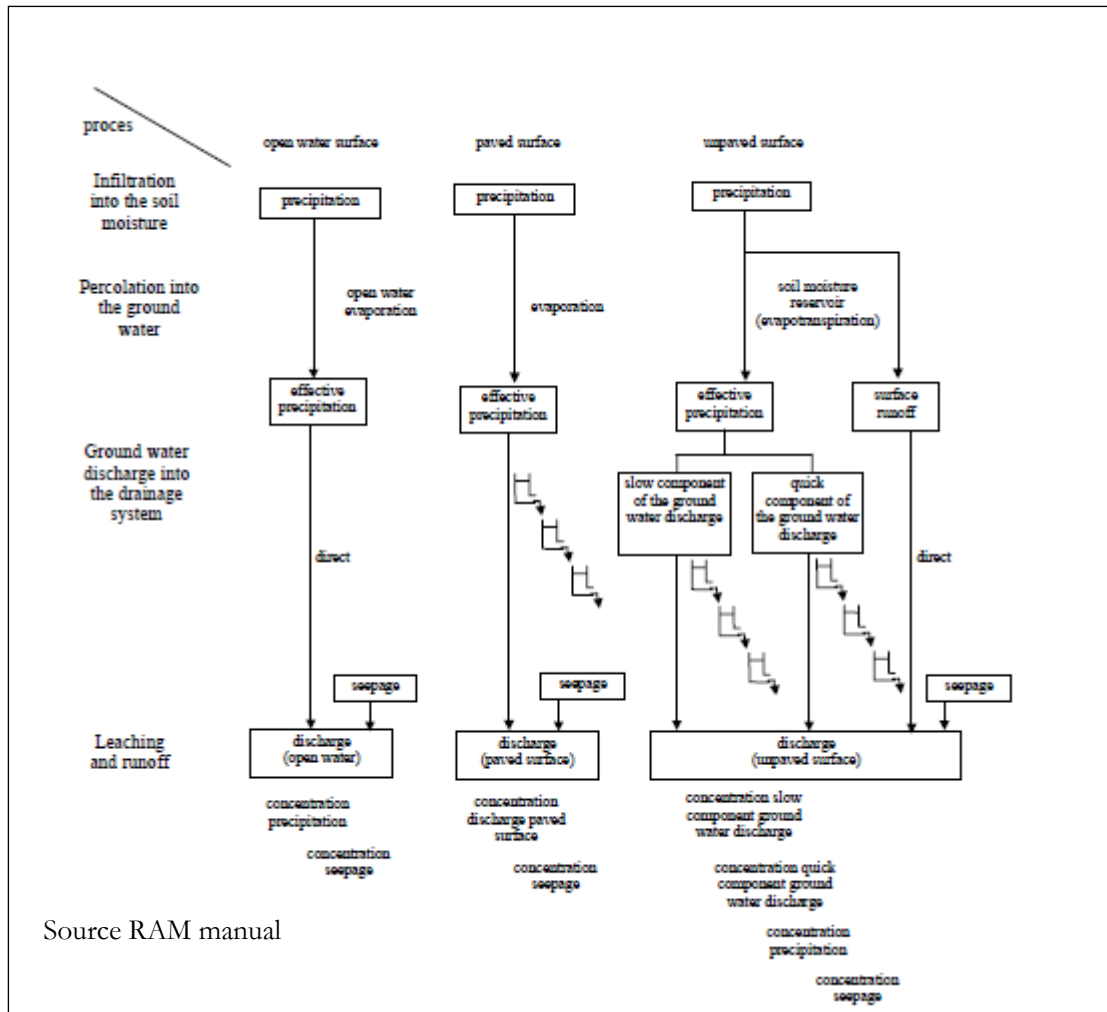


Figure 5-1 Duflow RAM modeling framework

The surfaces can be divided into three basic types.

- Open water surface
- Paved surface
- Unpaved surface

The linear reservoir model can be used to calculate runoff for each surface type. The calculation of runoff takes place in two stages. First the specific discharge [mm/day] per time interval is calculated, it defined as the discharge during the time interval $t-1$ to t . Secondly, the specific discharge converts to instantaneous discharge [m^3/s] at the end of time interval.

All model equations represented here is from the Duflow & RAM Manuals (DUFLOW-RAM, 2004).

5.3.1. Open water surface

The water bodies like rivers, lakes and reservoirs in a catchment can be considered as open water. The water lost in open water only by evaporation and almost directly by runoff.

$$P_{N,open_water,t} = P_{b,t} - f_0 E_{r,t} \quad 5-3$$

$$q_{open_water,t} = q_{open_water,t-1} e^{-\Delta t/k_0} + P_{N,open_water,t} (1 - e^{-\Delta t/k_0}) \quad 5-4$$

$$Q_{open_water,t} = a A_{open_water,t} q_{open_water,t} \quad 5-5$$

Where;

Input

$P_{b,t}$	[mm/day]	precipitation intensity
$E_{r,t}$	[mm/day]	reference crop evaporation Makkink
$q_{open_water,t-1}$	[mm/day]	specific discharge open water surface
$A_{open_water,t}$	[ha]	open water surface

Model parameters

f_0	[-]	crop factor Makkink for open water
k_0	[day]	time constant reservoir open water surface
Δt	[day]	time step
a	[-]	conversion factor units

Output

$P_{N,open_water,t}$	[mm/day]	effective precipitation open water surface
$Q_{open_water,t}$	[m ³ /s]	discharge open water surface

5.3.2. Paved surface

The paved area can further be divided into three parts as paved surface in a rural area, urban area and green house area. In this research, it can be assumed that the paved area is urban area (open paved surface) since the most of sub-catchment in the city of Enschede falls into that category. Precipitation in this area will partly fall on paved surface (roads, buildings) and be collected by the drainage system. Part of this precipitation will temporarily be stored and then evaporated. The governing equations are listed below.

$$I_{o,t} = P_{b,t} - f_0 E_{r,t} + \frac{B_{o,t-1}}{\Delta t} \quad 5-6$$

$$P_{N,o,t} = P_{b,t} - f_o E_{r,t} + \frac{B_{o,t-1}}{\Delta t} - I_{o,t} - \frac{B_{v,max}}{\Delta t} \quad 5-7$$

$$q_{o,o,t} = q_{o,o,t-1} e^{-\Delta t/k_{oo}} + P_{N,o,t} (1 - e^{-\Delta t/k_{oo}}) \quad 5-8$$

$$Q_{o,o,t} = a A_{o,o} q_{o,o,t} \quad 5-9$$

$$q_{o,i,t} = q_{o,i,t-1} e^{-\Delta t/k_{oi}} + I_{o,t} (1 - e^{-\Delta t/k_{oi}}) \quad 5-10$$

$$Q_{o,i,t} = aq_{o,i,t}(A_{o,r} + A_{o,o}) \quad 5-11$$

Where

Input

$P_{b,t}$	[mm/day]	precipitation intensity
$E_{r,t}$	[mm/day]	reference crop evaporation Makkink
$B_{o,t-1}$	[mm]	storage at open paved surface
$q_{o,o,t-1}$	[mm/day]	specific discharge other open paved surface
$q_{o,i,t-1}$	[mm/day]	specific discharge infiltrated water
$A_{o,o}$	[ha]	other open paved surface
$A_{o,r}$	[ha]	open paved surface with sewer system
$I_{i,o}$	[mm/day]	infiltration intensity open paved surface

Model parameters

f_0	[-]	crop factor Makkink for open water
$k_{o,o}$	[day]	time constant reservoir other open paved surface
$k_{o,i}$	[day]	time constant reservoir
$B_{v,max}$	[mm]	maximum storage at surface
Δt	[day]	time step
a	[-]	conversion factor units

Output

$I_{o,t}$	[mm/day]	infiltration intensity
$P_{N,o,t}$	[mm/day]	surface runoff at open paved surface
$q_{o,o,t-1}$	[mm/day]	specific discharge other open paved surface
$Q_{o,o,t}$	[m ³ /s]	discharge from other open paved surface
$Q_{o,i,t-1}$	[mm/day]	specific discharge infiltrated water

5.3.3. Unpaved surfaces

For the runoff of unpaved surface, three sub-processes are distinguished:

1. Infiltration into the soil moisture (unsaturated zone)
2. Percolation into groundwater (saturated zone)
3. Groundwater discharge via drainage system

The corresponding linear reservoir equations are listed below.

$$I_t = \Phi_{PF=0} - \Phi_{t-1} + P_{per,max} \quad 5-12$$

$$P_{N,sur,t} = P_{b,t} + \frac{B_t}{\Delta t} - I_t - \frac{B_{max}}{\Delta t} \quad 5-13$$

$$\Phi_t = \Phi_{t-1} + (I_t - E_{a,t} - P_{per,t})\Delta t \quad 5-14$$

$$q_{sur,t} = q_{sur,t-1}e^{-\Delta t/k_{sur}} + P_{N,sur,t}(1 - e^{-\Delta t/k_{sur}}) \quad 5-15$$

$$Q_{sur,t} = aA_{unpaved}q_{sur,t} \quad 5-16$$

Where

Input

$P_{b,t}$	[mm/day]	precipitation intensity
B_{t-1}	[mm]	storage in surface depressions
I_{t-1}	[mm/day]	infiltration intensity
Φ_{t-1}	[mm]	actual moisture storage at time t-1
$E_{a,t}$	[mm/day]	actual evapotranspiration
$P_{prec,t}$	[mm/day]	percolation into the saturated zone
$A_{unpaved}$	[ha]	unpaved surface

Model parameters

I_{max}	[mm/day]	infiltration capacity
Δt	[day]	time step
$P_{prec,max}$	[mm/day]	percolation into the saturated zone at PF=0
$\Phi_{pF=0}$	[mm]	moisture storage if pF=0
B_{max}	[mm]	maximum storage in surface depressions
K_{sur}	[day]	time constant reservoir surface runoff unpaved surface
a	[-]	conversion factor units

Output

I_t	[mm/day]	infiltration capacity
$P_{N,sur,t}$	[mm/day]	effective precipitation surface runoff
Φ_t	[mm]	actual moisture storage
$q_{sur,t}$	[mm/day]	specific surface runoff unpaved surface
$Q_{sur,t}$	[m ³ /s]	surface runoff unpaved surface

During the discharge through the saturated zone, the runoff can be divided into slow component and quick component, it occurs because of the different resistances in the soil. All components are modeled by linear reservoirs and the Figure 5-1 showed the whole processes of multiple linear reservoirs.

Following input parameter procedures, total runoff of sub-catchment has been calculated and was used as inflow data in DufLOW model.

5.4. Previous modeling studies with DufLOW

In the literature review it was found that some previous studies performed using DufLOW model as a simulation tool. Makkinga (1998) used DufLOW to model dissolved oxygen in the river Regge. Results indicated that DufLOW is a valuable tool for scenario analysis and a suitable tool to evaluate hydrology and pollution dynamics. Ochir (2008) also used DufLOW DMS effectively for the surface water quality assessment and modeling the Tuul River (Mongolia), and he also modeled the impacts of wastewater treatment plants. It showed a reasonable capability to reflect water quality using ammonium, nitrate, nitrite, DO, COD and BOD in DufLOW. Mwanuzi et al. (2003) used the DufLOW model to simulate the buffering process and capacity to absorb

sediments, nutrients and pollutants of the wetland in Lake Victoria. He conclude that the model represent a good agreement with the measured values on both hydrodynamics and water quality part.

5.5. Model simplifications and limitations

The precipitation runoff module in DMS is described at only one sub-catchment based on DEM, there is no water pumped from other sub-catchment, and the area average values was used as input data, however, in reality, water direction in urban area often changed by sewer system. Also the surface properties and parameter values vary from location to location. The option of course exists to create multiple RAM areas to better represent the land surface.

As a simple model the capillary rise from the ground water to the unsaturated zone were not considered and infiltration and percolation are made to immediately result in ground water recharge. Several parameters specified in the RAM module have no direct physical relevance and strongly conceptual and empirical in nature.

6. SIMPLIFIED “PROTOTYPE” DUFLOW–RAM MODELING

6.1. Modeling objectives

Hydrologic and water quality models are increasingly used to guide water resources strategies, water resources management and water resources regulation (Dingman, 2015). In this research, it was intended to use the model to simulate Enschede sub-discharge system under extreme precipitation. Furthermore, the results could be used to evaluate the functioning of Kristalbad. It was observed that the excess water overflow from the reservoir under extreme rainfall events, may affect the ability to store and treat water. Thus a numerical and schematization model could help designers and decision makers to re-examine the constructed wetland.

The modeling study is limited to Enschede sub-catchment having an area 4.3km². Modeling is performed with Duflow-RAM, and considering the availability of data, a simulation period was selected at 10th September 2013 and a 20 min time interval (temporal resolution) was selected for the analysis. Due to the fact that limited detailed data available for WWTP and Kristalbad, this study is set up as a simplified “prototype” model, which is not yet realistic, but it can be implemented and become more complex later on. This will be discussed later on in this chapter.

6.2. Schematization of the study area

For the modeling processes, the physical schematization is a significant part which is depends on the data availability and accuracy. In this sense, user can define the physical modeling details of study area. The following component shows the key points of Duflow physical model formulation.

- Nodes, schematization points
- Stream lines
- Cross-section definition
- RAM runoff areas modules
- Structures (weir, discharge point WWTP)

Nodes were set at some key positions such as junctions, outlets of the channels and both sides of structures. The steam sections were designed considering from the outlet of Enschede to WWTP. As a simply model all stream sections were assumed to same size and shape. The stream sections were considered to be trapezoidal. The rainfall runoff area (RAM) component was defined by following information.

- Surface classification and characterization
- Precipitation and Evapotranspiration (ET)
- Soil Parameters and surface properties

Practical catchments show more complexity and variability with respect to soil type, land cover, land use and topographic characteristics. In Duflow the sub-catchments are represented by RAM elements and provided average parameter values for each surface, and the surface classification was retrieved from the LULC map (Figure 4-9), there are 23,102m² of open water, 3,931,125m² of paved surfaces and 443,196m² of unpaved surface from total 4,397,425m² of whole sub-catchment, which is calculated as 0.5 %, 89.4 % and 10.1% of open water, paved and unpaved surfaces respectively. Besides we assumed paved surface consist of 60%, 1%, and 28.4% of sewer, green house and other paved surface as the urban properties. Figure 6-1 shows the result of the simulation.

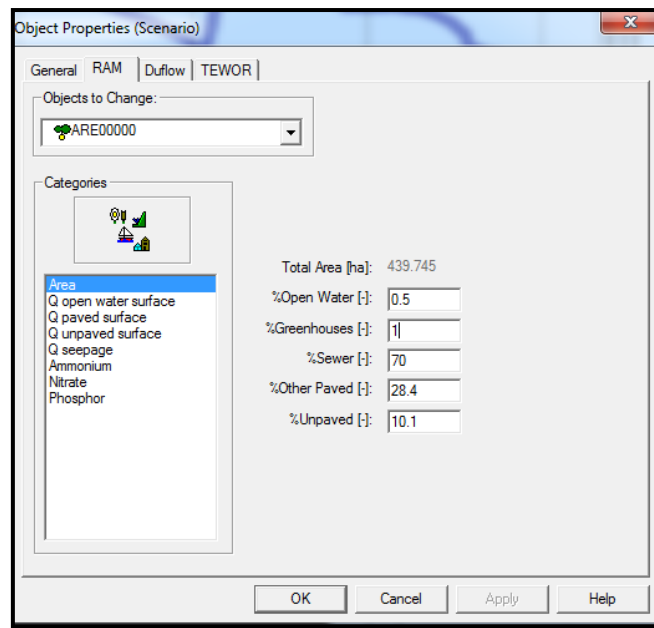


Figure 6-1 Percentage of each categories

6.3. Precipitation and Evaporation

Precipitation and evaporation schemes are the basic input parameters used in the RAM component. In this study, the precipitation data was available at 20 minutes intervals and hence daily calculation steps for flow were selected in the model simulations. The evaporation data was mean daily data from KNMI. In addition, there is a possibility in defining data using non-equidistant, constant and with Fourier time series settings. The example graph is shown in Figure 6-2. The other input parameters were defined in the respective menus. Duflow will automatically adjust the temporal variation for each parameter.

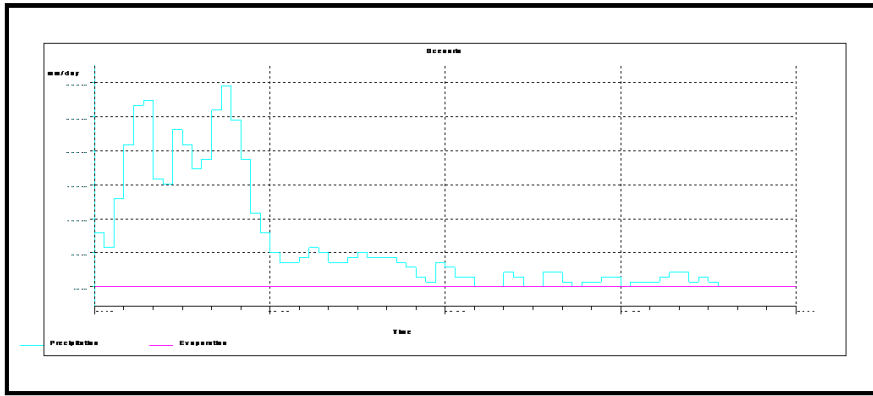


Figure 6-2 Time relate graph of precipitation and evaporation (mm/day) for RAM

6.4. Initial and Boundary conditions

Initial and boundary conditions are the most significant part for a numerical model at the beginning of simulation. The initial conditions represent the status of the model at the onset of the simulation period and normally it is difficult to estimate the true value at the initial state as this kind of information is hard to collect. This was the same even for this research and the data set required here are in form of water levels, discharges (Q), and depth of cross-sections. “It is often recommended practice to run the model for trial runs and to use the subsequent model run output as initial conditions” (Mwanuzi et al., 2003), but it was impractical to use this method and as such assumed a virtual network from Enschede to Kristalbad. Thus, the initial condition of discharge is set 0.01 and an initial condition of water level is set 24.75 and depth set as -1. This means Duflow will use water levels and not depth as state variable.

The boundary conditions are defined the physical boundaries and internal nodes of the system. At the upstream node, boundary conditions were set at a very low value to make sure to keep the streams wet, and a level boundary condition was set at the downstream end. There were no internal boundary conditions used but the RAM can be considered as boundary condition at the connected schematization point. In the RAM components, precipitation and evapotranspiration are the main boundary conditions which were defined as time series. Based on the boundary conditions and surface parameters RAM calculates the addition runoff flow as a Q_{add} scheme.

Urban surface characteristics (paved scheme)

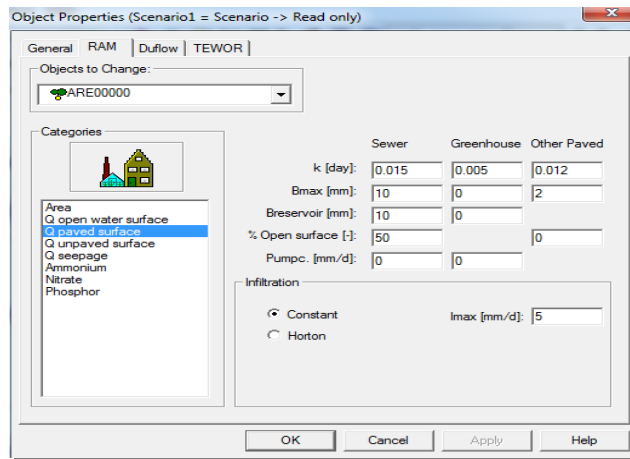


Figure 6-3 Urban surface characteristic

Soil surface characteristics (unpaved scheme)

Soil data extracted from the literature and some researches. It is defined in the unpaved scheme as follows:

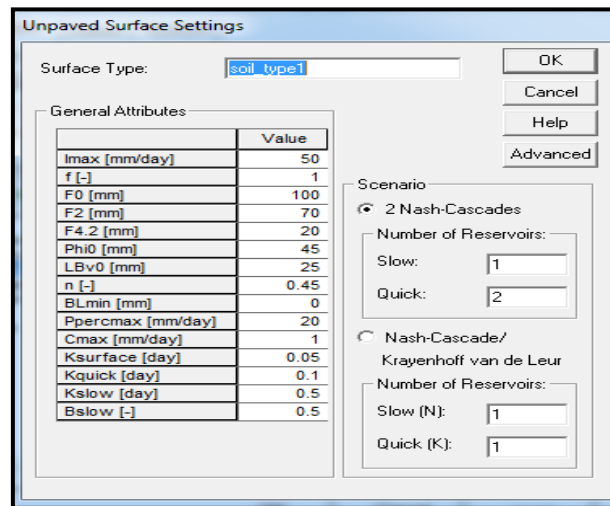


Figure 6-4 Unpaved surface scheme setting for study area

6.5. RAM simulation result

The simulation result shown in Figure 6-5, since it need some time to accumulate more water to form runoff, it shows the discharge lags behind at the beginning of time. The peak discharge was around $13\text{m}^3/\text{s}$ and the time of the peak of the discharge corresponds to that of the precipitation. It also can be found that water from paved surface make the most contribution to the discharge.

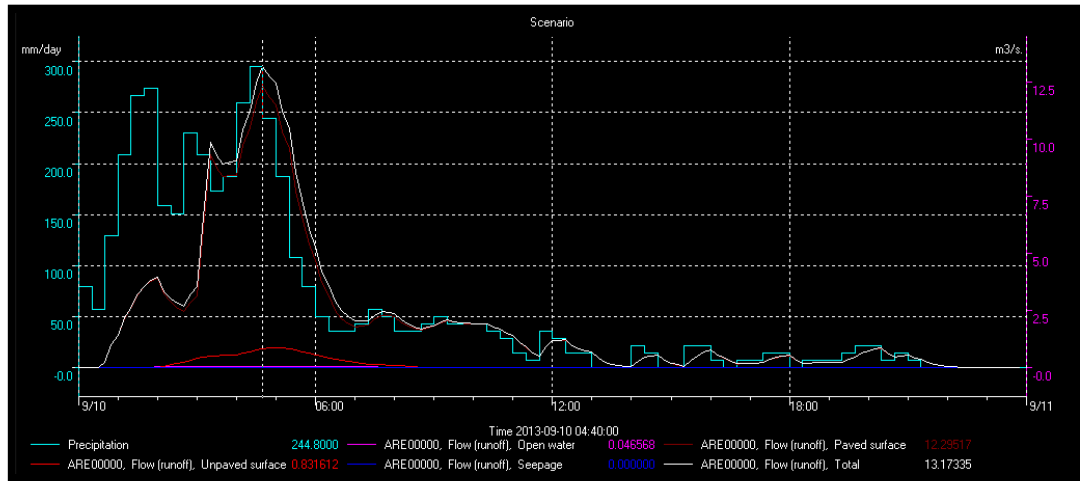


Figure 6-5 Discharge computed from RAM module

7. CONCLUSIONS AND RECOMMENDATIONS

7.1. Overall conclusions

A brief sequence of the entire study as implemented is described as below:

- Proposal writing
- Use of remote sensing for extreme rainfall monitoring and assessment
- Use of GIS (DEM, LULC data processing) to build and set-up urban hydrology and hydraulic models (acquire and pre-process input data)
- Prototype DMS model set-up (RAM and DMS network component)
- Conclusion and recommendations

This research was an initial research, starting up the application of remote sensing data, GIS and models for analysis of urban water management infrastructures, near Enschede (NL). From this study, the following conclusions can be drawn:

1. Use of satellite data for extreme rainfall

- The use of geostationary weather satellite data (Meteosat MSG) for monitoring extreme rainfall was investigated in this research, a specific event (leading to inundations and flash flooding in the streets in the center of Enschede city (20th June 2013) was selected as case study. The use of the MSG MPE or the MSG multisensory precipitation near real time estimate, accessible in near real time by GEONETCast systems, gives a good predication pattern of the storm behavior. However, the extreme rain rates are underestimated by the combined MW-IR algorithm. So, it is not entirely useful to get the good instantaneous rain rates for these weather conditions.
- Also another algorithm using MSG data, but based on the Cloud Physical Properties (CPP) and OCA data (optimal cloud analysis products from EUMETSAT) was evaluated. This algorithm is promising as after parameter calibration with rain gauge data, the extreme event could be simulated. The time interval of the data (15-minute MSG SEVIRI to 1- hour for OCA data) is however too large to evaluate these rapidly changing extreme rainfalls. It can be suggested to verify the use of the MSG-RSS (repaid scan service) delivering raw MSG SERIVI data in 5-minute periods over Europe)
- The older AE algorithm tested in this study, results showed it did not yield satisfactory results for estimating extreme rainfall over this region, and under these event circumstances.

It can be recommended to further analysis the use of RS data for extreme rainfall. In the Netherlands, also Ground weather Doppler Radar (from KNMI) data are a good potential source for rainfall estimation or a combination with satellite data.

2. Applicability of using remote sensing data for characterized the drainage area and network

- The SRTM-30m data used here are not suitable to delineate urban (and peri-urban) catchments in the region of Enshcede (NL). Even as the Enschede area has some relief (more than usual, compared to most regions in the west of the Netherlands), catchment delineation large errors are evident (see Figure 4-3&4-5) and in consequence also the drainage.
- The use of the AHN1 (5m) high resolution and especially the AHN2 (0.5m) very high resolution are more useful for delineating catchments and drainage networks. Elevations,

flow directions and location of channels correspond to real world conditions. We must however always bear in mind, that recent road building, hydraulic works, etc. may change patterns. Small elevation differences can induce large changes in networks, if not inspected. Field verification and consultation with the local or regional water management authorities will always be required to get the appropriate information on the urban and semi-urban drainage (because of the so many human interactions).

- The Ilwis DEM hydro-processing module is suitable for generating the drainage and network data, when good parameterization is done.

The TOP10NL data were used for characterizing the urban paved-unpaved land surface. Due to its precision, this is suitable as it is based on regular updates of the cadastral boundaries and land features (build-up, etc.).

It can be recommended to test the use of high resolution (+- 1 to 2 m) satellite imagery (WorldView-2, Pleiades, GeoEye, etc.) for obtaining the new (2015) land use land cover information. For example, the Kristalbad (constructed wetland area built in 2011-2013) is not yet implemented in the TOP10NL (Feb, 2015).

3. Applicability of the DMS-RAM model for Enschede urban runoff and drainage

- RAM is a conceptual but widely used tool to compute rainfall runoff from user defined catchment areas. The linear reservoir concept was developed and is widely used in the Netherlands also in other models like SOBEK, to model rainfall-runoff processes from land (and water) areas. Of course, today much more complex urban drainage models exist (Sobek, InfoWorks, 3Di, Wodan, etc.), but many are expensive commercial packages and not freely available.
- Full parameterization of the RAM component requires however more data and information then could be gathered during this short MSc study. A fully calibrated model could not be developed within the time limits of this MSc study. Therefore, only a very simple simulation, using the catchment delineation and drainage was performed and shown in this work.
- RAM allows to generate runoff flows (and water quality loadings), but parameter calibration is essential for an appropriate use. The following model settings can be derived from remote sensing information: Surface properties (distribution of paved, unpaved, water bodies, sewer, seepage, etc.). This leaves much information generation to the user who has to find other data sources:
 - Number of linear reservoir model setup (parallel, serial, # cascade,...) and the reservoir time constants (through calibration);
 - Soil properties (hydraulic and retention characteristic)
 - Water (in soil) and depression storages (and initial values);
 - Drainage and infiltration process rate constants;
 - Capillary rise (shallow groundwater);
- When sewers are present, RAM allows to pump runoff away (e.g. to a WWTP, or a CSO (combined sewer overflow system), but the user has to specify the pump capacity. Under free gravity drainage, rough estimations are needed to model sewers. These can only be found by calibration (from observed data, e.g. overflow spill structures or WWTP intake volumes, etc.).

4. Use of DMS Duflow (for modelling the water flows and quality, the WWTP outfall on the Elsbeek and Kristalbad)

- A prototype schematization of the WWTP – Elsbeek – Kristalbad was made, based upon data and information from the water authority (see Figure 7-1).
- DMS contains the necessary elements to construct a (1-D type) of model to simulate the behavior of the Kristalbad. The Kristalbad has however many hydraulic operating structures to manage the water flows through the 3 retention areas. We designed only 2 retention areas (as the last third is still under construction and not yet in full use).

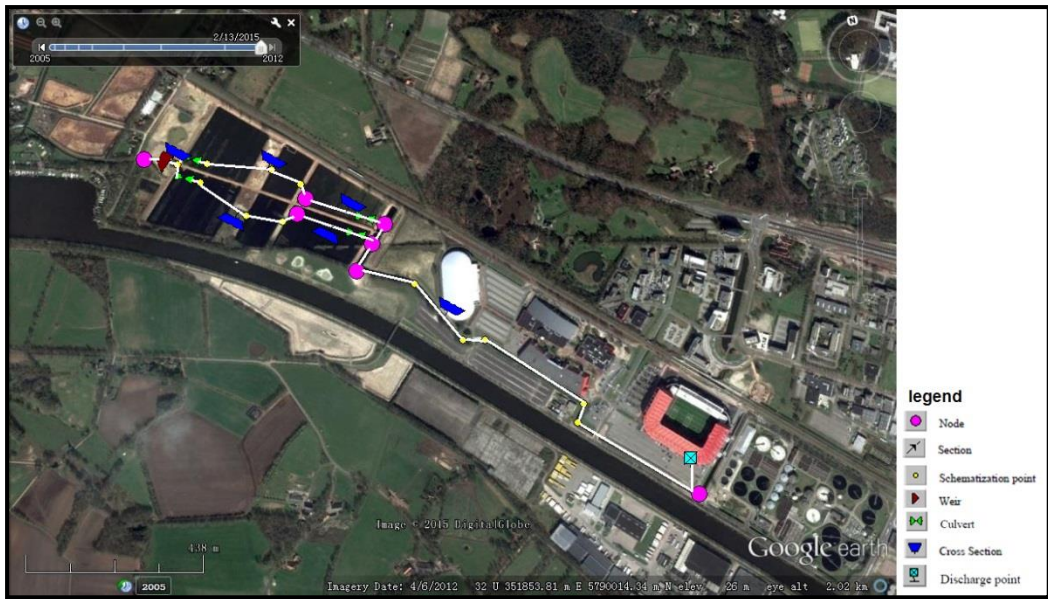


Figure 7-1 Example of network for Kristalbad

Due to time constraint of this MSc, detailed model runs could not be generated, as building a detailed physical scheme, required much topographic, design and local information. Also the operation (schemes) of the structures plays an important role in the flow through the system. Because Duflow is a 1-D model, it will be important to see whether this model, permits to simulate especially the water quality processes in the ponds (and is not over-simplified).

7.2. Recommendations

This first research revealed very much the complexity (and essential data requirements) of such urban and semi-urban water studies, and basically much more time and manpower is needed to analyze the behavior of urban water infrastructures under extreme rainfalls, including water quality. Urban drainage systems are very complex, with lots of manmade interventions and infrastructure, which all need due attention in order to evaluate the system behavior.

It is therefore suggested to follow-up this research in next MSc studies. First of all, it can be proposed to split the main overall subject into specific topic and parts for different researches. Satellite monitoring and forecasting of extreme rainfall can be a subject, as well as urban runoff modelling. Water quality assessment and modelling and e.g. assessment of the performance of constructed wetland type structures like the Kristalbad, also should be a subject, because it will require also water quality sampling and analysis.

REFERENCES

- Amorati, R., Alberoni, P. P., Levizzani, V., & Nanni, S. (2000). IR-based satellite and radar rainfall estimates of convective storms over northern Italy. *Meteorological Applications*, 7(1), 1–18. doi:10.1017/S1350482700001328
- Anagnostou, E. N., Negri, A. J., & Adler, R. F. (1999). A satellite infrared technique for diurnal rainfall variability studies. *Journal of Geophysical Research*, 104(D24), 31477. doi:10.1029/1999JD900157
- Arroyo, P., Blanco, I., Cortijo, R., De Luis Calabuig, E., & Ansola, G. (2013). Twelve-year performance of a constructed wetland for municipal wastewater treatment: Water quality improvement, metal distribution in wastewater, sediments, and vegetation. *Water, Air, and Soil Pollution*, 224(11), 1762. doi:10.1007/s11270-013-1762-3
- Beaumont, J., Clerbaux, N., Fettweis, X., & Erpicum, M. (2013). Rainfall retrieval using Spinning Enhanced Visible and Infrared Imager (SEVIRI-MSG) and Cloud Physical Properties (CPP) algorithm: validation over Belgium and applications. *Bulletin de La Société Géographique de Liège*, 61(2013-2). Retrieved from <http://orbi.ulg.ac.be/handle/2268/167811>
- Becker, A., & Grünewald, U. (2003). Disaster management. Flood risk in Central Europe. *Science (New York, N.Y.)*, 300(5622), 1099. doi:10.1126/science.1083624
- Beniston, M., Stephenson, D. B., Christensen, O. B., Ferro, C. A. T., Frei, C., Goyette, S., ... Woth, K. (2007). Future extreme events in European climate: an exploration of regional climate model projections. *Climatic Change*, 81(S1), 71–95. doi:10.1007/s10584-006-9226-z
- Berger, F. H. (2003). Meteosat-6 Rapid Scan IR/WV technique for estimating precipitation. *EGS - AGU - EUG Joint Assembly*. Retrieved from <http://adsabs.harvard.edu/abs/2003EAEJA....12822B>
- Brandsma, T. (2014). *Comparison of automatic and manual precipitation networks in the Netherlands* (p. 42p).
- Burrows, J. P., Borrell, P., & Platt, U. (Eds.). (2011). *The Remote Sensing of Tropospheric Composition from Space*. Berlin, Heidelberg: Springer Berlin Heidelberg. doi:10.1007/978-3-642-14791-3
- Clemmens, A. J., Holly, F. M., & Schuurmans, W. (1993). Description and Evaluation of Program: Duflow. *Journal of Irrigation and Drainage Engineering*, 119(4), 724–734. doi:10.1061/(ASCE)0733-9437(1993)119:4(724)
- D.M.A. Aminou. (2002). MSG's SEVIRI instrument. *ESA Bulletin*, 111, 15–17.
- Davies, C. M., & Bavor, H. J. (2000). The fate of stormwater-associated bacteria in constructed wetland and water pollution control pond systems. *Journal of Applied Microbiology*, 89(2), 349–60. Retrieved from <http://www.ncbi.nlm.nih.gov/pubmed/10971769>

- Dingman, S. L. (2015). *Physical Hydrology: Third Edition* (p. 643). Waveland Press. Retrieved from <https://books.google.com/books?id=rUUaBgAAQBAJ&pgis=1>
- DUFLOW. (2004). *Duflow Modelling Studio:RAM manual Precipitation Runoff Module* (V3.7,Stowa ed.).
- DUFLOW-RAM. (2004). *Duflow Modelling Studio RAM manual Precipitation Runoff Module* (V3.7,Stowa ed.).
- EUMETSAT. (2010). Optimal Cloud Analysis Factsheet. *EUM/OPS/DOC/09/5175*, (v1A). Retrieved from <http://www.eumetsat.int>
- Farr, T. G., Rosen, P. A., Caro, E., Crippen, R., Duren, R., Hensley, S., ... Alsdorf, D. (2007). The Shuttle Radar Topography Mission. *Reviews of Geophysics*, 45(2), RG2004. doi:10.1029/2005RG000183
- García, M., Soto, F., González, J. M., & Bécares, E. (2008). A comparison of bacterial removal efficiencies in constructed wetlands and algae-based systems. *Ecological Engineering*, 32(3), 238–243. doi:10.1016/j.ecoleng.2007.11.012
- Groisman, P. Y., Knight, R. W., Easterling, D. R., Karl, T. R., Hegerl, G. C., & Razuvaev, V. N. (2005). Trends in Intense Precipitation in the Climate Record. *Journal of Climate*, 18(9), 1326–1350. doi:10.1175/JCLI3339.1
- Hartmann, D. L., Tank, A. M. G. K., Rusticucci, M., Alexander, L. V., S. Brönnimann, Y. Charabi, F. J. D., Dlugokencky, E. J., ... P.W. Thorne, M. W. and P. M. Z. (2013). Observations: Atmosphere and Surface. In V. B. and P. M. M. Stocker, T.F., D. Qin, G.-K. Plattner, M. Tignor, S.K. Allen, J. Boschung, A. Nauels, Y. Xia (Ed.), *Climate Change 2013: The Physical Science Basis. Contribution of Working Group I to the Fifth Assessment Report of the Intergovernmental Panel on Climate Change* (pp. 159–254). Cambridge University Press. doi:10.1017/CBO9781107415324.008
- Heinemann, T. (2002). The Eumetsat multi-sensor precipitation estimate (MPE). ... *Working Group (IPWG)* Retrieved from http://oiswww.eumetsat.int/~idders/html/doc/IPWG_2002_MPE.pdf
- KNMI. (n.d.). Retrieved August 22, 2014, from http://www.knmi.nl/over_het_knmi/kennisinstituut.html
- Levizzani, V. (2002). A review of satellite-based rainfall estimation methods. ... *Project MUSIC Report* (.... Retrieved from http://www.researchgate.net/publication/252272255_A_Review_of_Satellite-based_Rainfall_Estimation_Methods/file/72e7e521c97febcea0.pdf
- Maathuis, B. H. P., & Wang, L. (2006). Digital Elevation Model Based Hydro-processing. *Geocarto International*, 21(1), 21–26. doi:10.1080/10106040608542370
- Makkinga AA ,Nieuwenhuis RA, A. R. (1998). Modelling dissolved oxygen in the river Reggae system using Duflow. *European Water Management : Official Publication of the European Water Pollution Control Association*, 1(1), 37 – 42.

- Meteosat Second Generation. (n.d.). Retrieved August 21, 2014, from http://www.esa.int/Our_Activities/Observing_the_Earth/Meteosat_Second_Generation/How_M_SG_works
- Mwanuzi, F., Aalderink, H., & Mdamo, L. (2003). Simulation of pollution buffering capacity of wetlands fringing the Lake Victoria. *Environment International*, 29(1), 95–103. doi:10.1016/S0160-4120(02)00150-2
- Nauss, T., & Kokhanovsky, A. A. (2007). Assignment of rainfall confidence values using multispectral satellite data at mid-latitudes: first results. *Advances in Geosciences*, 10, 99–102. Retrieved from <https://hal.archives-ouvertes.fr/hal-00296984/>
- Ochir, A. (2008). Surface water quality assessment and modelling a case study on the Tuul river, Ulaanbaatar city, Mongolia. *ITC, Enschede*, 87pp.
- Peel, M. C., Finlayson, B. L., & McMahon, T. A. (2007). Updated world map of the Köppen-Geiger climate classification. *Hydrology and Earth System Sciences*, 11(5), 1633–1644. doi:10.5194/hess-11-1633-2007
- Roebeling, R. A., Feijt, A. J., & Stammes, P. (2006). Cloud property retrievals for climate monitoring: Implications of differences between Spinning Enhanced Visible and Infrared Imager (SEVIRI) on METEOSAT-8 and Advanced Very High Resolution Radiometer (AVHRR) on NOAA-17. *Journal of Geophysical Research*, 111(D20), D20210. doi:10.1029/2005JD006990
- Roebeling, R. A., & Holleman, I. (2009). SEVIRI rainfall retrieval and validation using weather radar observations. *Journal of Geophysical Research*, 114(D21), D21202. doi:10.1029/2009JD012102
- Roebeling, R. A., & van Meijgaard, E. (2009). Evaluation of the Daylight Cycle of Model-Predicted Cloud Amount and Condensed Water Path over Europe with Observations from MSG SEVIRI. *Journal of Climate*, 22(7), 1749–1766. doi:10.1175/2008JCLI2391.1
- Roebeling, R. A., Wolters, E. L. A., Meirink, J. F., & Leijnse, H. (2012). Triple Collocation of Summer Precipitation Retrievals from SEVIRI over Europe with Gridded Rain Gauge and Weather Radar Data. *Journal of Hydrometeorology*, 13(5), 1552–1566. doi:10.1175/JHM-D-11-089.1
- Rosenfeld, D., & Gutman, G. (1994). Retrieving microphysical properties near the tops of potential rain clouds by multispectral analysis of AVHRR data. *Atmospheric Research*, 34(1-4), 259–283. doi:10.1016/0169-8095(94)90096-5
- Rutger, D., & Rpland, H. (2008, March 13). Extreme Temperatures and Precipitation in Europe: Analysis of a High-Resolution Climate Change Scenario. OPOCE. Retrieved from <http://publications.jrc.ec.europa.eu/repository/handle/111111111/589>
- Schmetz, J., Pili, P., Tjemkes, S., Just, D., Kerkmann, J., Rota, S., & Ratier, A. (2002). Supplement to An Introduction to Meteosat Second Generation (MSG). *Bulletin of the American Meteorological Society*, 83(7), 991–991. doi:10.1175/BAMS-83-7-Schmetz-1

- Scofield, R. A., & Kuligowski, R. J. (2003). Status and Outlook of Operational Satellite Precipitation Algorithms for Extreme-Precipitation Events. *Weather and Forecasting*, 18(6), 1037–1051. doi:10.1175/1520-0434(2003)018<1037:SAOOOS>2.0.CO;2
- Semmler, T., & Jacob, D. (2004). Modeling extreme precipitation events—a climate change simulation for Europe. *Global and Planetary Change*, 44(1-4), 119–127. doi:10.1016/j.gloplacha.2004.06.008
- Stephens, G. L., Paltridge, G. W., & Platt, C. M. R. (1978). Radiation Profiles in Extended Water Clouds. III: Observations. *Journal of the Atmospheric Sciences*, 35(11), 2133–2141. doi:10.1175/1520-0469(1978)0352.0.CO;2
- Subramanya, K. (2009). *Flow in Open Channels* (p. 548). Tata McGraw-Hill Education. Retrieved from https://books.google.com/books?id=haljh3BO_1IC&pgis=1
- Thomas Heinemann, J. K. (2003). The EUMETSAT Multi Sensor Precipitation Estimate (MPE): Concept and Validation. Retrieved from <http://citeseerx.ist.psu.edu/viewdoc/summary?doi=10.1.1.9.3917>
- Vicente, G. A., Scofield, R. A., & Menzel, W. P. (1998). The Operational GOES Infrared Rainfall Estimation Technique. *Bulletin of the American Meteorological Society*, 79(9), 1883–1898. doi:10.1175/1520-0477(1998)079<1883:TOGIRE>2.0.CO;2
- Wentz, F. J., & Spencer, R. W. (1998). SSM/I Rain Retrievals within a Unified All-Weather Ocean Algorithm. *Journal of the Atmospheric Sciences*, 55(9), 1613–1627. doi:10.1175/1520-0469(1998)055<1613:SIRRWA>2.0.CO;2
- Yucel, I., & Onen, A. (2014). Evaluating a mesoscale atmosphere model and a satellite-based algorithm in estimating extreme rainfall events in northwestern Turkey. *Natural Hazards and Earth System Sciences*, 14, 611–624. doi:10.5194/nhess-14-611-2014

APPENDIX

Appendix 1 Raw data import into ILWIS format

Geospatial Data Abstraction Library (GDAL) information

C:\GDAL\bin\gdalinfo input map (the map is in grib format)

GDAL_translate

```
@echo off
```

```
echo rem: MSG MPEF OCA time series UMARF dataset import to ilwis
```

```
rem source data from UMARF archive
```

```
rem note different file naming from EUMETCast reception
```

```
echo rem: sample file name = MSG3-SEVI-MSGOCAE-0100-0100-20130620000000.000000000Z-1109892.grb
```

```
rem pick timestamp from long filename
```

```
set longfilename=%1
```

```
set shortfilename1=%longfilename:~28,10%
```

```
rem watch your program paths this batch code needs
```

```
set PATH=%C:\B2_rainfall2014\Ilwis372_Jan2014\Extensions\GEONETCast-Toolbox\GDAL\bin%
```

```
call gdal_translate.exe -of ilwis MSG3-SEVI-MSGOCAE-0100-0100-20130620000000.000000000Z-1109892.grb
```

```
MSG_OCAE_%shortfilename1%
```

```
rem set PATH=%C:\B2_rainfall2014\Ilwis372_Jan2014%
```

```
rem call Ilwis.exe -C setgrf safr_%shortfilename1%.mpr lst_south
```

```
rem set undefined values to ? (ilwis) and create maplist according file info in header (use gdalinfo)
```

```
call Ilwis.exe -C MSG_OCAE_%shortfilename1%_undef.mpl:=maplistcalculate("iff(@1 ne
```

```
9999,@1,?)",0,11,MSG_OCAE_%shortfilename1%.mpr);
```

```
rem delete unused files
```

```
rem del HDF5_LSASAF_MSG_DMET_NAfr_%shortfilename1%.*
```

```
rem view results
```

```
rem call ilwis.exe open
```

Appendix 2 Map calculation

These scripts compute all the map lists of cloud properties and rain rate

```
CWP:=2*10^(re_COT_1)*10^6*re_cer_1/3
```

```
re_CTH.mpl:=maplistapplic(twente_CTT.mpl,"(292.4-##)/5.5")
```

```
re_NL_CTH:=(NL_cth_1+nL_cth_2+nL_cth_3+nL_cth_4)/4
```

```
RR_1:=(cwp_1/160-1)^2/7.62
```

```
R_EX.mpl:=maplistapplic(re_hour_CTT.mpl,"(1.1183*10^11*exp(-0.036382*##^1.2))")
```

Appendix 3 Rain rate (mm/h) of each point retrieved from MSG on June 20th 2013

time	WWTP	KNMI	ENSCHEDÉ	TWENTE	p1	p2	p3
1	0	0	0	0.01014	0	0	0
2	0	0	0	0.010143	0	0	0
3	0	0	0	0.010141	0	0	0
4	0	0	0	0.010132	0	0	0
5	0	0	0	0.010139	0	0	0
6	0	0	0	0.010136	0	0	0
7	0	0	0	0.010135	0	0	0
8	0	0	0	0.01014	0	0	0
9	0	0	0	0.010139	0	0	0
10	0	0	0	0.010129	0	0	0
11	0.0144	0	0	0.010118	0	0	0
12	5.2272	2.3616	5.76	0.010108	6.984	2.088	1.4256
13	8.5248	12.8304	12.2688	12.11012	9.576	11.7936	7.0848
14	2.0016	2.5056	2.4624	15.71014	2.3616	2.2032	2.808
15	0.216	0.3024	0.1728	3.810107	0.1872	0.3024	0.2448
16	0.1584	0.1728	0.2016	0	0.1728	0.1728	0.2016
17	0	0	0	0.010098	0	0	0
18	0	0	0	0.010106	0	0	0
19	0	0	0	0.010104	0	0	0
20	0	0	0	0.010096	0	0	0
21	0	0	0	0.010087	0	0	0
22	0	0	0	0.010096	0	0	0
23	0	0	0	0	0	0	0
24	0	0	0	0	0	0	0
sum	16.1424	18.1728	20.8656	31.81255	19.2816	16.56	11.7648

Appendix 4 Rain rate (mm/h) retrieved from AE and CPP during daylight

Daylight	AE	CPP	Rain gauge
10:00	0.059	0.000	0.01
11:00	0.563	0.000	0.01
12:00	7.136	0.000	0.01
13:00	22.599	7.594	12.11
14:00	17.295	16.185	15.71
15:00	8.323	7.918	3.81
16:00	6	0.000	0.00
17:00	1.989	0.000	0.01
sum	63.964	31.697	31.67

Appendix 5 Rain rate, level and discharge data for WWTP (source: Water authority)

USE OF SATELLITE DATA TO MONITOR URBAN WATER MANAGEMENT INFRASTRUCTURES
UNDER EXTREME WEATHER CONDITIONS: PRELIMINARY STUDY

Time	rainfall	level	head	discharge
	mm	mNAP	mNAP	m3/s
10/09/2013 00:00	0,7	25,739	28,000	0,000
10/09/2013 00:20	1,1	25,739	28,000	0,000
10/09/2013 00:40	0,8	25,739	28,000	0,000
10/09/2013 01:00	1,8	25,739	28,000	0,000
10/09/2013 01:20	2,9	25,739	28,000	0,000
10/09/2013 01:40	3,7	25,739	28,000	0,000
10/09/2013 02:00	3,8	25,739	28,000	0,000
10/09/2013 02:20	2,2	25,739	28,000	0,000
10/09/2013 02:40	2,1	25,739	28,000	0,000
10/09/2013 03:00	3,2	25,739	28,000	0,000
10/09/2013 03:20	2,9	26,303	28,000	0,000
10/09/2013 03:40	2,4	27,519	28,000	1,175
10/09/2013 04:00	2,6	28,185	28,000	2,815
10/09/2013 04:20	3,6	28,221	28,000	3,653
10/09/2013 04:40	4,1	28,238	28,000	4,063
10/09/2013 05:00	3,4	28,239	28,000	4,096
10/09/2013 05:20	2,6	28,239	28,000	4,107
10/09/2013 05:40	1,5	28,239	28,000	4,115
10/09/2013 06:00	1,1	28,236	28,000	4,011
10/09/2013 06:20	0,7	28,225	28,000	3,746
10/09/2013 06:40	0,5	28,210	28,000	3,397
10/09/2013 07:00	0,5	28,194	28,000	3,001
10/09/2013 07:20	0,6	28,172	28,000	2,518
10/09/2013 07:40	0,8	28,151	28,000	2,065
10/09/2013 08:00	0,7	28,128	28,000	1,623
10/09/2013 08:20	0,5	28,102	28,000	1,153
10/09/2013 08:40	0,5	28,078	28,000	0,776
10/09/2013 09:00	0,6	28,061	28,000	0,534
10/09/2013 09:20	0,7	28,050	28,000	0,398
10/09/2013 09:40	0,6	28,042	28,000	0,304
10/09/2013 10:00	0,6	28,035	28,000	0,226
10/09/2013 10:20	0,6	28,027	28,000	0,160
10/09/2013 10:40	0,5	28,020	28,000	0,097
10/09/2013 11:00	0,4	28,017	28,000	0,079
10/09/2013 11:20	0,2	28,015	28,000	0,066
10/09/2013 11:40	0,1	28,014	28,000	0,060
10/09/2013 12:00	0,5	28,014	28,000	0,056
10/09/2013 12:20	0,4	28,010	28,000	0,037
10/09/2013 12:40	0,2	28,003	28,000	0,011
10/09/2013 13:00	0,2	27,992	28,000	0,001
10/09/2013 13:20	0,0	27,984	28,000	0,000
10/09/2013 13:40	0,0	27,980	28,000	0,000
10/09/2013 14:00	0,0	27,975	28,000	0,000
10/09/2013 14:20	0,3	27,931	28,000	0,000
10/09/2013 14:40	0,2	27,858	28,000	0,000
10/09/2013 15:00	0,0	27,756	28,000	0,000
10/09/2013 15:20	0,0	27,603	28,000	0,000
10/09/2013 15:40	0,3	27,373	28,000	0,000
10/09/2013 16:00	0,3	27,091	28,000	0,000
10/09/2013 16:20	0,1	26,791	28,000	0,000
10/09/2013 16:40	0,0	26,488	28,000	0,000
10/09/2013 17:00	0,1	26,190	28,000	0,000
10/09/2013 17:20	0,1	25,913	28,000	0,000
10/09/2013 17:40	0,2	25,760	28,000	0,000
10/09/2013 18:00	0,2	25,737	28,000	0,000
10/09/2013 18:20	0,0	25,737	28,000	0,000
10/09/2013 18:40	0,1	25,737	28,000	0,000
10/09/2013 19:00	0,1	25,737	28,000	0,000
10/09/2013 19:20	0,1	25,738	28,000	0,000
10/09/2013 19:40	0,2	25,738	28,000	0,000
10/09/2013 20:00	0,3	25,738	28,000	0,000
10/09/2013 20:20	0,3	25,738	28,000	0,000
10/09/2013 20:40	0,1	25,738	28,000	0,000
10/09/2013 21:00	0,2	25,738	28,000	0,000
10/09/2013 21:20	0,1	25,738	28,000	0,000

USE OF SATELLITE DATA TO MONITOR URBAN WATER MANAGEMENT INFRASTRUCTURES
UNDER EXTREME WEATHER CONDITIONS: PRELIMINARY STUDY

10/09/2013 21:40	0,0	25,738	28,000	0,000
10/09/2013 22:00	0,0	25,738	28,000	0,000
10/09/2013 22:20	0,0	25,737	28,000	0,000
10/09/2013 22:40	0,0	25,737	28,000	0,000
10/09/2013 23:00	0,0	25,737	28,000	0,000
10/09/2013 23:20	0,0	25,737	28,000	0,000
10/09/2013 23:40	0,0	25,737	28,000	0,000

Appendix 6 Inlet of level and discharge data for Kristalbad (source: Water authority)

time	level	Q1+2
	mNAP	m3/s
10/09/2013 00:00	24,284	0,556
10/09/2013 00:20	24,298	0,490
10/09/2013 00:40	24,316	0,390
10/09/2013 01:00	24,337	0,291
10/09/2013 01:20	24,356	0,230
10/09/2013 01:40	24,371	0,269
10/09/2013 02:00	24,381	0,296
10/09/2013 02:20	24,387	0,311
10/09/2013 02:40	24,390	0,321
10/09/2013 03:00	24,392	0,325
10/09/2013 03:20	24,394	0,331
10/09/2013 03:40	24,397	0,341
10/09/2013 04:00	24,402	0,354
10/09/2013 04:20	24,405	0,364
10/09/2013 04:40	24,408	0,372
10/09/2013 05:00	24,436	0,461
10/09/2013 05:20	24,493	0,652
10/09/2013 05:40	24,519	0,747
10/09/2013 06:00	24,537	0,815
10/09/2013 06:20	24,543	0,838
10/09/2013 06:40	24,547	0,855
10/09/2013 07:00	24,549	0,863
10/09/2013 07:20	24,544	0,845
10/09/2013 07:40	24,532	0,797
10/09/2013 08:00	24,512	0,721
10/09/2013 08:20	24,496	0,665
10/09/2013 08:40	24,483	0,617
10/09/2013 09:00	24,470	0,572
10/09/2013 09:20	24,458	0,531
10/09/2013 09:40	24,446	0,491
10/09/2013 10:00	24,435	0,456
10/09/2013 10:20	24,427	0,431
10/09/2013 10:40	24,421	0,412
10/09/2013 11:00	24,415	0,395
10/09/2013 11:20	24,411	0,383
10/09/2013 11:40	24,408	0,373
10/09/2013 12:00	24,404	0,362
10/09/2013 12:20	24,402	0,356
10/09/2013 12:40	24,401	0,353
10/09/2013 13:00	24,401	0,352
10/09/2013 13:20	24,400	0,350
10/09/2013 13:40	24,399	0,348
10/09/2013 14:00	24,397	0,342
10/09/2013 14:20	24,395	0,335
10/09/2013 14:40	24,392	0,326
10/09/2013 15:00	24,389	0,318
10/09/2013 15:20	24,386	0,311
10/09/2013 15:40	24,382	0,300
10/09/2013 16:00	24,378	0,289
10/09/2013 16:20	24,375	0,281
10/09/2013 16:40	24,375	0,280
10/09/2013 17:00	24,383	0,300
10/09/2013 17:20	24,389	0,318
10/09/2013 17:40	24,389	0,318

USE OF SATELLITE DATA TO MONITOR URBAN WATER MANAGEMENT INFRASTRUCTURES
UNDER EXTREME WEATHER CONDITIONS: PRELIMINARY STUDY

10/09/2013 18:00	24,388	0,316
10/09/2013 18:20	24,388	0,315
10/09/2013 18:40	24,389	0,317
10/09/2013 19:00	24,389	0,318
10/09/2013 19:20	24,389	0,318
10/09/2013 19:40	24,388	0,316
10/09/2013 20:00	24,385	0,306
10/09/2013 20:20	24,380	0,292
10/09/2013 20:40	24,377	0,284
10/09/2013 21:00	24,375	0,279
10/09/2013 21:20	24,372	0,271
10/09/2013 21:40	24,368	0,260
10/09/2013 22:00	24,364	0,251
10/09/2013 22:20	24,361	0,243
10/09/2013 22:40	24,359	0,237
10/09/2013 23:00	24,357	0,233
10/09/2013 23:20	24,358	0,234
10/09/2013 23:40	24,358	0,235

Appendix 7 Outlet of level data (source: Water authority)

time	mNAP
10/09/2013 00:00	22,784
10/09/2013 00:20	22,781
10/09/2013 00:40	22,782
10/09/2013 01:00	22,784
10/09/2013 01:20	22,789
10/09/2013 01:40	22,795
10/09/2013 02:00	22,806
10/09/2013 02:20	22,823
10/09/2013 02:40	22,846
10/09/2013 03:00	22,875
10/09/2013 03:20	22,911
10/09/2013 03:40	22,953
10/09/2013 04:00	22,998
10/09/2013 04:20	23,044
10/09/2013 04:40	23,090
10/09/2013 05:00	23,136
10/09/2013 05:20	23,193
10/09/2013 05:40	23,248
10/09/2013 06:00	23,341
10/09/2013 06:20	23,464
10/09/2013 06:40	23,626
10/09/2013 07:00	23,756
10/09/2013 07:20	23,855
10/09/2013 07:40	23,934
10/09/2013 08:00	23,993
10/09/2013 08:20	24,023
10/09/2013 08:40	24,041
10/09/2013 09:00	24,049
10/09/2013 09:20	24,050
10/09/2013 09:40	24,048
10/09/2013 10:00	24,041
10/09/2013 10:20	24,032
10/09/2013 10:40	24,023
10/09/2013 11:00	24,013
10/09/2013 11:20	24,004
10/09/2013 11:40	23,995
10/09/2013 12:00	23,986
10/09/2013 12:20	23,978
10/09/2013 12:40	23,970
10/09/2013 13:00	23,962
10/09/2013 13:20	23,956
10/09/2013 13:40	23,950
10/09/2013 14:00	23,944
10/09/2013 14:20	23,939

10/09/2013 14:40	23,933
10/09/2013 15:00	23,926
10/09/2013 15:20	23,919
10/09/2013 15:40	23,911
10/09/2013 16:00	23,896
10/09/2013 16:20	23,875
10/09/2013 16:40	23,851
10/09/2013 17:00	23,829
10/09/2013 17:20	23,810
10/09/2013 17:40	23,794
10/09/2013 18:00	23,780
10/09/2013 18:20	23,767
10/09/2013 18:40	23,755
10/09/2013 19:00	23,743
10/09/2013 19:20	23,733
10/09/2013 19:40	23,724
10/09/2013 20:00	23,716
10/09/2013 20:20	23,709
10/09/2013 20:40	23,701
10/09/2013 21:00	23,692
10/09/2013 21:20	23,684
10/09/2013 21:40	23,676
10/09/2013 22:00	23,667
10/09/2013 22:20	23,657
10/09/2013 22:40	23,648
10/09/2013 23:00	23,639
10/09/2013 23:20	23,629
10/09/2013 23:40	23,621

Appendix 8 More details about Kristalbad

